Kinetic investigations of combustion of small oxygenated aliphatic hydrocarbons – modeling and experiments

Capriolo, Gianluca

2020

Document Version:
Publisher's PDF, also known as Version of record

Kinetic investigations of combustion of small oxygenated aliphatic hydrocarbons – modeling and experiments

GIANLUCA CAPRIOLO
DIVISION OF COMBUSTION PHYSICS | DEPARTMENT OF PHYSICS | LUND UNIVERSITY

Kinetic investigations of combustion of small oxygenated aliphatic hydrocarbons – modeling and experiments

Kinetic investigations of combustion of small oxygenated aliphatic hydrocarbons – modeling and experiments

Gianluca Capriolo

LUND
UNIVERSITY

DOCTORAL DISSERTATION

by due permission of the Faculty of Engineering, Lund University, Sweden.
To be defended at Rydsbergsalen, Fysicum, Professorsgatan 1.
12th June 2020 at 13:15.

Faculty opponent
Prof. Peter Glarborg, Department of Chemical and Biochemical Engineering, CHEC. Research Centre, Technical University of Denmark, DK.

Organization LUND UNIVERSITY Division of Combustion Physics, Department of Physics P.O. Box 118, SE-211 00 Lund, Sweden	Document name: Doctoral Dissertation
	Date of issue June 12, 2020
Author: Gianluca Capriolo	Sponsoring organization

Title:
Kinetic investigations of combustion of small oxygenated aliphatic hydrocarbons – modeling and experiments

Abstract

The depletion of oil reserves and the increasingly stringent European Union regulation of air pollution have forced researchers and manufacturers to search for cleaner and sustainable substitutes to petroleum-based transportation fuels. Biofuels like small aliphatic alcohols are of increasing interest as alternatives to fossil fuels, as they offer long-term fuel-source regenerability. As major advantages, bio-alcohols promise to reduce environmental impact and to be ready-to-use, as their employment requires minor adjustments in internal combustion engines. However, only methanol and ethanol have established themselves on the fuel market, while the use of higher homologous is still a research matter. To this end, to make a proper selection of alternative fuels, the main aim of the thesis was to increase the understanding of chemical reaction networks of propyl alcohols combustion. The thesis focused on building a detailed kinetic reaction model capable to predict the decomposition and oxidation processes, as well as the formation of undesired and harmful pollutant, such as NO. Kinetic investigation also included the study of propanal, which is a critical stable intermediate derived from the oxidation of 1-propanol. Moreover, my research was also comprehensive of the experimental investigation of NO formation in methanol flames. The combustion kinetic models developed during my PhD studies were assessed against both new and available burning velocities, as well as against other combustion properties performed with different devices and methods from literature.

New laminar burning measurements were performed at atmospheric pressure and different temperature using the heat flux method.

NO predictions from the kinetic model were assessed against new quantitative NO mole fraction measurements in the post-flame region. Experiments were performed using saturated laser-induced fluorescence and flames were stabilized using the heat flux burner.

The presented combustion models were also compared with the most reliable models from literature and the strengths and weaknesses in the combustion chemistry predictions of such mechanisms were evaluated and discussed.

Key words:
Buofuels, Kinetic Modelling, laminar burning velocity, Propanal, n-Propanolo, i-propanol, Laser-Induced Fluorescence diagnostics, Nitric oxide.

Classification system and/or index terms (if any)

Supplementary bibliographical information		Language: English
ISSN and key title		ISBN 978-91-7895-504-6 (print) ISBN 978-91-7895-505-3 (pdf)
Recipient's notes	Number of pages: 71	Price
	Security classification	

Signature 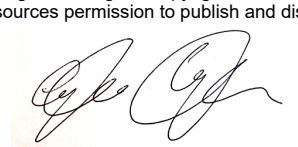 Date 2019-04-30

Kinetic investigations of combustion of small oxygenated aliphatic hydrocarbons – modeling and experiments

Gianluca Capriolo

LUND
UNIVERSITY

Faculty of Engineering
Department of Physics
Lund University

ISBN 978-91-7895-504-6 (print)
ISBN 978-91-7895-505-3 (pdf)

Printed in Sweden by Media-Tryck, Lund University
Lund 2020

“Surely a tall drink of water like yourself
can put out a few flames”

Carlos Oliveira, RE 3 (2020)

Table of contents

Abstract

The depletion of oil reserves and the increasingly stringent European Union regulation of air pollution have forced researchers and manufacturers to search for cleaner and sustainable substitutes to petroleum-based transportation fuels. Biofuels like small aliphatic alcohols are of increasing interest as alternatives to fossil fuels, as they offer long-term fuel-source regenerability. As major advantages, bio-alcohols promise to reduce environmental impact and to be ready-to-use, as their employment requires minor adjustments in internal combustion engines. However, only methanol and ethanol have established themselves on the fuel market, while the use of higher homologous is still a research matter. To this end, to make a proper selection of alternative fuels, the main aim of the thesis was to increase the understanding of chemical reaction networks of propyl alcohols combustion. The thesis focused on building a detailed kinetic reaction model capable to predict the decomposition and oxidation processes, as well as the formation of undesired and harmful pollutant, such as NO. Kinetic investigation also included the study of propanal, which is a critical stable intermediate derived from the oxidation of 1-propanol. Moreover, my research was also comprehensive of the experimental investigation of NO formation in methanol flames. The combustion kinetic models developed during my PhD studies were assessed against both new and available burning velocities, as well as against other combustion properties performed with different devices and methods from literature.

New laminar burning measurements were performed at atmospheric pressure and different temperature using the heat flux method.

NO predictions from the kinetic model were assessed against new quantitative NO mole fraction measurements in the post-flame region. Experiments were performed using saturated laser-induced fluorescence and flames were stabilized using the heat flux burner.

The presented combustion models were also compared with the most reliable models from literature and the strengths and weaknesses in the combustion chemistry predictions of such mechanisms were evaluated and discussed.

Popular Summary

"We need for a *sustainable alternative* to the finiteness of the fossil fuels", that's the leitmotif sentence recurring worldwide since several decades. In this regard, the word sustainable was not used at random. In fact, global warming, greenhouse gases and pollution emissions have led the combustion community to a massive response (much like a Pavlovian conditioning) to obtain cleaner and lasting alternatives to petroleum derivatives fuels . In this context, biofuels can be employed as fuels/fuel additives, as their combustion properties allow them to be used in internal combustion engines without significant design modifications and, above all, because they have showed promising benefits in terms of reducing pollutant emissions. However, it is important to ascertain whether the combustion of biofuels does not lead to the formation of unwanted by-products, which might have detrimental effects on human health. In this sense, the development of reliable, detailed kinetic mechanisms is a key aspect that can allow the understanding and prediction of the dynamics on the combustion processes of potential alternative fuels. A detailed kinetic model tends to mimic what truly happens into the combustion process, i.e., every chemical transformation is described exactly in the way is expected to happen.

Reliability and robustness of kinetic models are usually tested against a wide range of new or literature experiments performed at different combustion regimes, and this was the cornerstone of my doctoral research. More precisely, the primary aim of my PhD project was to increase the understanding of combustion characteristics of propyl alcohols, which are promising biofuels, as well as of one of the major intermediates derived from the oxidation of n-propanol, i.e., propanal. To this end, new detailed propyl alcohols and propanal combustion kinetic models were developed and assessed against new experimental and literature data.

The experimental investigations involved the determination of the laminar burning velocity (LBV), a key parameters of premixed flames that provide invaluable information about the combustion characteristics of the fuel-mixture which, in turn, can be used, in developing detailed kinetic model, or, on a more practical point of view, to design combustion devices.

The secondary, but not less important, goal of my research was to investigate on the formation of one of the most harmful pollutants derived from combustion of fossil fuels, namely nitric oxide (NO) in methanol and propanol isomers flames. Nitrogen oxides (NO_x) emissions have a very detrimental effect on the environment, contributing, among others, to the cause of the ozone depletion and acid rains. Besides, it is also proved that they have deleterious effects on human health as well, being the cause of severe respiratory pathologies by virtue of their toxic and disruptive action on the lungs airway epithelium. Regarding this, NO is the most abundant species presents in NO_x emissions. That said, improving the understanding

related to the NO formation in methanol and propyl alcohols flames (which are among the most important alternative fuel candidates) via accurate measurements, and subsequent development of appropriate kinetic models, is a crucial step for designing cleaner combustion engines.

The new detailed kinetic models developed during my research showed very good agreements in representing the experimental data and can be considered a benchmark model for the investigated biofuels. In addition, I believe that the new experimental data provided during my doctoral research will be of great help for the combustion modellers to further refine kinetic mechanisms.

List of papers

Paper I. G. Capriolo, V.A. Alekseev, A.A. Konnov, *An experimental and kinetic study of propanal oxidation*, Combust. Flame 197 (2018) 11-21.

This work provides new laminar burning velocity, LBV, measurements of propanal + air mixture at 298, 323, 343, and 393 K, under atmospheric pressure using heat flux method. A new detailed kinetic model for propanal combustion was also proposed and validate against the new LBV results and also literature data performed at different regimes. Moreover, the proposed kinetic model was compared with the predictions of semi-detailed Politecnico di Milano. Data inconsistencies that have been arisen among the new and literature LBVs data, as well as differences between models simulations, were analysed and discussed.

I was responsible for performing the LBV measurements. Propanal kinetic subset was developed together with prof. A.A. Konnov, while I wrote the scientific article with the contribution of my co-authors.

Paper II. C. Brackmann, T. Methling, M. Lubrano Lavadera, G. Capriolo, A.A. Konnov, *Experimental and modeling study of nitric oxide formation in premixed methanol + air flames*, Combust. Flame 213 (2020) 322-330.

In this work were provided new quantitative nitric oxide mole fractions measurements in premixed laminar methanol + air flames in the post-combustion zone and the results were employed to assess six kinetic models from literature. Measurements were performed using saturated laser-induced fluorescence, flames were stabilized on a heat flux burner while the experimental investigations were set to 318 K, 1 atm and at $\phi = 0.7–1.5$.

I contributed in performing the experimental measurements together with the co-authors.

Paper III. G. Capriolo, A.A. Konnov, *Combustion of propanol isomers: experimental and kinetic modelling study*, Combust. Flame, under review.

In this study new experimental and kinetic modeling study combustion of propyl alcohols was conducted. New laminar burning velocity measurements were obtained using the heat flux method over the initial gas temperature range of 323–393 K and under atmospheric conditions. Data consistency of the new and available literature was verified through the analysis of the temperature dependence and differences were discussed. A new kinetic mechanism was also proposed and assessed against new and all available literature data obtained at different combustion regimes.

I was responsible for performing the LBV measurements. Propyl alcohols kinetic subset, as well as the writing of the manuscript, was developed together with prof. A.A. Konnov.

Paper IV. G. Capriolo, C. Brackmann, M. Lubrano Lavadera, T. Methling, A.A. Konnov, *An experimental and kinetic modelling study on nitric oxide formation in premixed C_3 alcohols flames*, Proc. Combust. Inst., under review (accepted for oral presentation at the 38th Int. Symp. on Combustion).

In this work are provided new quantitative nitric oxide, NO, mole fraction concentrations measurements in C_3 alcohols + air flames, together with a new detailed combustion kinetic mechanism. Flames were stabilized using the heat flux method and the initial gas conditions were set to 323 K, 1 atm and Φ=0.7-1.4. Saturated laser-induced fluorescence was employed to measure NO mole fraction in the post-combustion region. The presented and the available literature models, i.e. the POLIMI and Bohon kinetic models, were validated against the new provided experimental data.

Experimental measurements were performed with the contribution of the co-authors. The kinetic subset was developed together with prof. A.A. Konnov, while I wrote the scientific article with the contribution of my co-authors.

Related work

1. L. Dupont, H.Q. Do, G. Capriolo, A.A. Konnov, A. El Bakali, *Experimental and kinetic modeling study of para-xylene chemistry in laminar premixed flames*, Fuel 239 (2019) 814-29.
2. M. Lubrano Lavadera, C. Brackmann, G. Capriolo, T.Methling, A. A. Konnov, *Measurements of the laminar burning velocities and NO concentrations in neat and blended ethanol and n-heptane flames*, Fuel, under review.

1 Introduction

"Humanity's acquisition of better and more complex form of life, as associated with the expansion of knowledge, political and civil liberties, economic well-being and technical expertise".

This is one of the many ways in which *progress* can be defined, a word so invaluable to mankind that has become the *key aspect* that fuels the scientific research. In the combustion community, progress means, among others, scientific innovations aimed at improving the engineering of internal combustion devices, lowering pollutant emissions, as well as at proposing alternatives to fossil fuels. To reach such achievements, the development of comprehensive and reliable kinetic mechanisms is a critical step that allows improving the understanding of combustion processes.

1.1 Outline of the thesis

The outline of the thesis is as follow:

Chapter 2 explains the key role played by detailed combustion models in improving the characterization of the physicochemical properties of the transportation fuels, as well as in understanding their combustion properties. A brief discussion about the mechanisms of NO formation, as well as the sources and classification of kinetic model uncertainties, were also reported.

Chapter 3 provides information regarding laminar burning velocity definition and measurements. Particularly, the most important methodologies used to determine laminar burning velocity are briefly discussed and the attention was focused on the method employed during my doctoral studies, namely the heat flux method.

Chapter 4 concerns the laser-Induced Fluorescence technique and the experimental setup employed to quantify the NO formation in methanol and propanols flames.

Chapter 5 highlights the most important results obtained during my doctoral work.

2 Chemical kinetics

A *combustion kinetic model* includes species and the related thermodynamic and transport properties, as well as the elementary reactions, the associated rate constants and *third-body* collision efficiencies.

Compiling a kinetic mechanism might be quite challenging, especially for biofuel candidates, due to the lack of experimental and theoretical kinetic rate coefficient investigations. Moreover, the prediction of rate constants can be further complicated by the lack of knowledge about potential energy surface (PES), quantum states, anharmonicity and third-body collision efficiency, involves having a number of variables that exceed the number of equations, resulting in an indeterminate system [1].

Once a kinetic model has been built, its reliability and robustness is usually tested against a wide range of experiments performed at different combustion regimes, i.e., flames, shock tubes (STs), rapid compression machines (RCMs), flow reactors (FRs), jet stirred reactors (JSRs) etc. Chemically reacting mixtures are modeled by employing open source (Flamemaster [2], Cantera [3], Opensmoke [4, 5]), as well as proprietary (Chemkin [6], LOGEsoft [7], Cosilab [8], Chemical Workbench [9]) simulation software. The numerical tools, used to solve the series of differential equations that govern the combustion of the reactant mixture, i.e., conservation of mass, momentum, energy and species, will require setting initial and boundary conditions, and the resulting computational effort will depend on the combustion property investigated. For 0 dimensional experiments (ST, FT, JSR, RCM), the combustion process depends only on time, leading to low computational complexity. On the contrary, for multi-dimensional experiments, i.e., flames investigations, transport of species are rate limiting and need to be included in the calculation, which considerably increases the computational time required to run a simulation. In fact, for flames, the most important species dictating the reactivity is usually hydrogen atom, as it is the lightest radical present into the chemical reaction zone; such a characteristic allow it to immediately diffuse towards the unburned gases [10].

2.1 Rate expressions

The simplest way to describe a chemical reaction process is by representing it via an overall stoichiometric global equation, e.g., for oxidation of methane:

$$CH_4 + 2O_2 = CO_2 + 2H_2O \quad (1.1)$$

However, one-step reactions are rather rare in real processes. In most cases, the reaction proceeds via a sequence of elementary steps where intermediates (short-lived species with high reaction rate such as atoms and/or radicals) are produced. These intermediates react with each other and the reactants, and the final products are formed at the end. Each individual step is denoted as an *elementary reaction*.

Given an elementary bimolecular reaction:

$$aA + bB = cC + dD \quad (1.2)$$

The reversibility of the reaction allows us to find a rate of the forward reaction:

$$r_f = k_f[A]^a[B]^b \quad (1.3)$$

As well as a rate of the reverse reaction:

$$r_r = k_r[C]^c[D]^d \quad (1.4)$$

The rate coefficient k can be expressed as:

$$k = Ae^{-\left(\frac{E_a}{RT}\right)} \quad (1.5)$$

Or as:

$$k = AT^n e^{-\left(\frac{E_a}{RT}\right)} \quad (1.6)$$

Eq. (1.5) is known as Arrhenius form, while Eq. (1.6) is known as modified Arrhenius form.

Here:

A is the *pre-exponential factor*, which depends on frequency of collision and on steric (or probability) factor. A is calculated through the determination on the entropy of activation via the transition state theory (TST) [11].

n is the *temperature exponent*.

E_a is the *activation energy*, which is the minimum amount of energy required by chemical reactants to undergo a chemical reaction [12]. E_a is usually determined via quantum chemistry calculations.

k and A factor units are the same and are related to the overall reaction order, specifically s^{-1} for a first order reaction, $cm^3mol^{-1}s^{-1}$ for a second order reaction, $cm^6mol^{-2}s^{-1}$ for a third order reaction.

At the equilibrium the forward and reverse rates are equal:

$$r_f = r_r \tag{1.7}$$

Then, it is possible to define the *thermodynamic equilibrium constant* k_p, as follow:

$$k_p = \frac{k_f}{k_r} = \frac{[C]^c[D]^d}{[A]^a[B]^b} \tag{1.8}$$

Since the Gibbs free energy of reaction, ΔG_r, can be defined as $\Delta G_r = -RTln(k_p)$, if k_f and the thermodynamic data of the reacting species are known, is possible to calculate k_r.

2.1.1 Pressure-dependent reactions

Rate coefficients isomerization reactions and/or thermal decomposition of some small hydrocarbons can be pressure dependent. In case of intermediate pressures, the reaction rate of unimolecular reactions is neither second-order nor first-order. The simple way to derive the apparent first-order rate coefficient in this pressure region ("*fall-off region*", see Fig.1) is via the *Lindemann formalism* [13]; such an approach requires knowing Arrhenius rate parameters for both the low- and high-pressure limiting cases, which allows determining a pressure-dependent rate equation.

Given an unimolecular elementary reaction

$$AB = P \tag{1.9}$$

The overall process can be split in two steps:

$$AB + M \overset{k_1, k_{-1}}{\Longleftrightarrow} AB^* + M \tag{1.10}$$

$$AB^* + M \overset{k_2}{\Rightarrow} P \tag{1.11}$$

In the first bimolecular step, the collision between a bath gas molecule M (also known as *third-body),* and the reactant AB, transfers enough energy for AB to achieve a state that overcomes the reaction barrier (excitation step) [14]. This energized state AB^* can then either give the final product P or lose energy in a subsequent collision to reform AB (deactivation). At the steady-state concentration, $[AB]$ is constant, or, in other words,

$$\frac{d[AB]}{dt} = 0 \tag{1.12}$$

Assuming that the time required to reach the steady-state condition is negligible if compared to the total reaction time, the unimolecular rate constant, k_u, can be expressed as:

$$k_u = \frac{dP}{dt} = \frac{k_1 k_2 [M]}{k_{-1}[M] + k_2} [AB] \tag{1.13}$$

It is possible to identify two limiting cases of low, $[M] \to 0$, and high, $[M] \to \infty$, pressures.

For $[M] \to 0, k_{-1}[M] \ll k_2,$ Eq.(1.6) and Eq.(1.13) can be expressed, respectively, as follows:

$$k_0 = A_0 T^{n_0} e^{-\left(\frac{E_{a_0}}{RT}\right)} \tag{1.14}$$

$$k_u \to k_{u_0} = k_0 = k_1[M][AB] \tag{1.15}$$

This latter corresponds to a second order reaction. The rate-determining step is the first step, i.e., Eq. (1.10).

For $[M] \to \infty$, $k_{-1}[M] \gg k_2$, then:

$$k_\infty = A_\infty T^{n_\infty} e^{-\left(\frac{E_{a_\infty}}{RT}\right)} \tag{1.16}$$

$$k_u \to k_{u_\infty} = k_\infty = \frac{k_1 k_2}{k_{-1}} [AB] \tag{1.17}$$

That corresponds to a first order reaction. The rate-determining step is the second step, i.e., Eq. (1.11).

N_2 is usually used as bath gas in the experiments, so it is assumed to have unit collision efficiency and all of the other species are compared against it.

The *Troe formalism* [15] provides a more accurate approach to derive the apparent first-order rate coefficient in the intermediate pressure (fall-off) range:

$$k = k_\infty \left(\frac{P_r}{1+P_r}\right) F \tag{1.18}$$

Where the reduced pressure, P_r, is given by:

$$P_r = \frac{k_0}{k_\infty}[M] \tag{1.19}$$

The broadening factor, F, is expressed as:

$$logF = logF_{cent}\left\{1 + \left[\frac{logP_r + c}{n - d(logP_r + c)}\right]^2\right\}^{-1} \tag{1.20}$$

With: $c = -0.4 - 0.67 logF_{cent}$, $n = -0.75 - 1.271 logF_{cent}$ and $d = 0.14$

The *F-center* value, F_{cent} , defines the center of the fall-off range and is given by:

$$F_{cent} = (1-\alpha)e^{\left(-\frac{T}{T^{***}}\right)} + e^{\alpha\left(-\frac{T}{T^{*}}\right)} + e^{\left(-\frac{T^{**}}{T}\right)} \tag{1.21}$$

and the parameters α, T^{***}, T^{*}, T^{**} has to be determined in order to represent the fall-off curve.

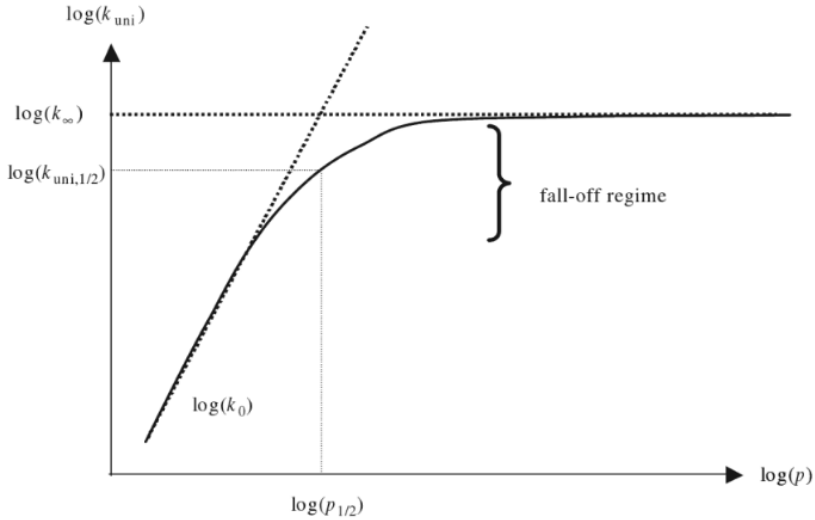

Fig.1. Schematic fall-off plot of the pressure dependence for a unimolecular rate constant, reprinted from [16].

The Troe formalism gives an accurate representation of the fall-off region for single-well PESs; however in case of elementary reactions with multiple wells(PES will have several minima for reactants, products and transition states for the species *activated*), the differences between the Troe fit and the rate coefficient calculated with a theoretical approach can be as high as 40%, leading to adoption of the so called "PLOG" formalism, e.g., see [17]:

$$logk_u(T,P_i) = logk_{u,i} + (logP - logP_i)\frac{logk_{u,i+1} - logk_{u,i}}{logP_{i+1} - logP_i} \quad (1.22)$$

With $i = 1, \ldots, N$

The *PLOG* fit is superior to the Troe one if the gas mixture composition does not change; however, in case of a change in the third-body efficiency of the mixture, it might result in an erroneous evaluation of the rate coefficient [10].

2.2 Developing a detailed kinetic model

2.2.1 The hierarchical approach

A detailed combustion kinetic mechanism is built to give a comprehensive representation of physical reality and to improve the understanding of combustion processes. However, there are several ways that can be used to develop a detailed kinetic model. The most common way (and also the one used to develop the kinetic mechanisms during my PhD studies) is to use the *hierarchical approach*. Here, the large model is hierarchically assembled on the basis of several sub-mechanisms built upon each other, starting on the one comprehending smaller species. This strategy allows the modeler to avoid to building the entire model from scratch but rather than to develop only the sub-mechanism of the targeted species and to add it, as a LEGO brick, on an already validated *core*, i.e., the base mechanism.

2.2.2 Low, intermediate and high temperature kinetic models

For hydrocarbons oxidation, it is possible to distinguish three distinct temperatures, i.e., low (600-750 K), intermediate (900-1250 K) and high temperature (>1300K) [10] at which correspond three different chemical behavior. This brought modelers which deal with the development of large kinetic mechanisms to (usually) present two different types of detailed mechanisms:

- A high temperature mechanism, suitable for flame modeling where diffusion effects have to be taking into account.
- Low and intermediate temperature mechanism, usually very large and complex, which is comprehensive of the addition to oxygen of alkyl radicals.

2.2.3 Reaction classes in detailed model

As already stated, one of the reason that can make challenging the developing of a proper detailed mechanism is the lack of studies associated to the rate coefficients determination. One way to circumvent this obstacle is to design reaction classes. The crucial aspect of reaction classes is that the rate coefficient is determined only using a local set of functional features around the *reactive center* (atoms involved in the reaction) [18].

According to Sarathy et al. [19] reaction classes are defined and listed as follow:

High temperature reaction classes:

- Unimolecular fuel decomposition
- H-atom abstraction from the fuel
- Alkyl radical decomposition
- Alkyl radical isomerization
- H-atom abstraction reactions from alkenes
- Addition of radical species $\ddot{O}$ and $\cdot OH$ to alkenes
- Reactions of alkenyl radicals with HO_2 ·, $\cdot CH_3O_2$, and $\cdot C_2H_5O_2$
- Alkenyl radical decomposition
- Alkene decomposition
- Retroene decomposition reactions

Low-temperature reaction classes:

- Addition of O_2 to alkyl radicals $R\cdot + O_2 = ROO\cdot$
- $R\cdot + ROO\cdot = RO\cdot + RO\cdot$
- $R\cdot + HO_2\cdot = RO\cdot + \cdot OH$
- $R\cdot + CH_3OO\cdot = RO\cdot + CH_3O\cdot$
- Alkyl peroxy radical isomerization $ROO\cdot = \cdot QOOH$
- Concerted eliminations $ROO\cdot = alkene = HO_2\cdot$
- $ROO\cdot + HO_2\cdot = ROOH + HO_2$
- $ROO\cdot + H_2O_2 = ROOH + HO_2\cdot$
- $ROO\cdot + CH_3O_2\cdot = RO\cdot + CH_3O\cdot + O_2$
- $ROO\cdot + ROO\cdot = RO\cdot + RO\cdot + O_2$
- $ROOH = RO\cdot + \cdot OH$
- $RO\cdot$ decomposition
- $QOOH = cyclic\ ether + \cdot OH$ (cyclic ether formation)
- $QOOH = alkene + \cdot HO_2$ (radical site β to OOH group)
- $QOOH = alkene + carbonyl + OH$ (radical site γ to OOH group)
- Addition of O_2 to $\cdot QOOH$ ($\cdot QOOH + O_2 = \cdot OOQOOH$)
- Isomerization of $\cdot OOQOOH$ and formation of keto-hydroperoxide ($HOOCH_2OCHO$) and $\cdot OH$
- Decomposition of ketohydroperoxide to form oxygenated radical species and $\cdot OH$
- Cyclic ether reactions with $\cdot OH$ and $\cdot HO_2$
- Decomposition of large carbonyl species and carbonyl radicals.

2.3 Mechanisms of NO Formation

Nitric oxide (NO) is one of the principal pollutants derived from combustion processes. By virtue of what has been stated, it is fundamental to understand the NO formation kinetics in the combustion system. There are three main chemical mechanisms for NO formation, namely thermal-NO, prompt-NO, and N_2O mechanisms.

2.3.1 Thermal NO

The thermal NO mechanism (usually referred also as *Zel'dovich* mechanism) consists of three reactions [20]:

$$N_2 + O \rightarrow NO + N \quad \text{(R1)}$$

$$O_2 + N \rightarrow NO + O \quad \text{(R2)}$$

$$N + OH \rightarrow NO + H \quad \text{(R3)}$$

Here, the rate-controlling is the reaction (R1), which requires breaking the bond of the stable species N_2 (the activation energy is around 75 kcal mol^{-1} [21, 22]) and then is favored at high-temperature conditions (>1800K). Also, NO formation is weakly subordinate to the availability of O_2; consequently, the NO emission peaks from derived internal combustion engines are reached slightly before stoichiometric conditions [20].

2.3.2 Prompt-NO

The presence of a further mechanism leading to NO production was identified by Fenimore [23] whereas the Zel'dovich mechanism was not able to reproduce NO formation. Prompt-NO can be formed in a conspicuous quantity at fuel-rich conditions and in turbulent diffusion flames [24].

The most important reaction involved into prompt-NO formation is:

$$CH + N_2 = \mathrm{NCN} + \mathrm{H} \quad \text{(R4)}$$

Here, (R4) is then the initiation step, proceeding via insertion of CH into the N_2 triple bond reaction to give NCN and H [25-27].

At high pressure conditions, the recombination reaction forming HNCN become also important [25]:

$$CH + N_2 = \text{HNCN} \quad \text{(R5)}$$

Other important reactions involved into prompt-NO formation, according to Glarborg et al. [99], are:

$$CN + N = C + N_2 \quad \text{(R6)}$$

$$C_2 + N_2 = 2CN \quad \text{(R7)}$$

$$NCN + M = C + N_2 + M \quad \text{(R8)}$$

$$NCN + H = HCN + N \quad \text{(R9)}$$

$$NCN + H = HNC + N \quad \text{(R10)}$$

$$NCN + O = CN + NO \quad \text{(R11)}$$

$$NCN + OH = HCN + NO \quad \text{(R12)}$$

$$NCN + OH = NCO + NH \quad \text{(R13)}$$

$$NCN + O_2 = NCO + NO \quad \text{(R14)}$$

$$NCN + NO = CN + N_2O \quad \text{(R15)}$$

2.3.3 The N_2O mechanism

The formation of NO through the N_2O route, according to Glarborg et al. [22], mainly involves the following reactions:

$$N_2 + O + M = N_2O + M \quad \text{(R16)}$$

$$N_2O + H = N_2 + OH \quad \text{(R17)}$$

$$NH + NO = N_2O + H \quad \text{(R18)}$$

$$N_2O + O = NO + NO \quad \text{(R19)}$$

$$N_2O + O = N_2 + H_2 \quad \text{(R20)}$$

Since the initiation step (R16) requires O atom and the three-body recombination reaction, NO formation is enhanced as air concentration and pressure increase [97].

2.3.4 NO-reburning

The NO-reburning route is an important strategy adopted in some combustion systems to reduce NO formation, especially under fuel-rich condition [22]. The NO-reburning route involves the presence of hydrocarbon radical which will react fast with NO contributing to its reduction in the combustion products.

Several reactions are implicated in the NO-reburning route; the main ones, according to the model of [22], are listed as follow:

$$CH_3 + NO = HCN + H_2O \quad \text{(R21)}$$

$$CH_3 + NO = H_2CN + OH \quad \text{(R22)}$$

$$^3CH_2 + NO = HCNO + H \quad \text{(R23)}$$

$$^3CH_2 + NO = HCN + OH \quad \text{(R24)}$$

$$^1CH_2 + NO = HCN + OH \quad \text{(R25)}$$

$$^1CH_2 + NO = {}^3CH_2 + NO \quad \text{(R26)}$$

$$CH + NO = CO + NH \quad \text{(R27)}$$

$$CH + NO = NCO + H \quad \text{(R28)}$$

$$CH + NO = HCN + O \quad \text{(R29)}$$

$$CH + NO = CN + OH \quad \text{(R30)}$$

$$CH + NO = HCO + N \quad \text{(R31)}$$

$$C + NO = CN + O \quad \text{(R32)}$$

$$C + NO = CO + N \quad \text{(R33)}$$

$$C_2H_3 + NO = HCN + CH_2O \quad \text{(R34)}$$

$$C_2H + NO = HCN + CO \quad \text{(R35)}$$

$$C_2H + NO = CN + HCO \quad \text{(R36)}$$

$$C_2 + NO = C_2O + N \quad \text{(R37)}$$

$$HCCO + NO = HCNO + CO \quad \text{(R38)}$$

$$HCCO + NO = HCN + CO_2 \quad \text{(R39)}$$

$$C_2O + NO = CO + NCO \quad \text{(R40)}$$

$$HCNO + H = HCN + OH \quad \text{(R41)}$$

$$HCNO + O = HCO + NO \quad \text{(R42)}$$

$$HCNO + O = NCO + OH \quad \text{(R43)}$$

$$HCNO + OH = CO + H_2NO \quad \text{(R44)}$$

$$HCNO + OH = HCO + HNO \quad \text{(R45)}$$

2.4 Sensitivity analysis and uncertainty quantification in chemical kinetic mechanisms

Sensitivity analysis is a very powerful tool that not only allows to identify the key reactions implicated in the (pyrolysis and/or oxidation) processes, but even which elementary reactions affect global or local combustion property, e.g., the impact of the reactions on the species concentration or temperature. The act of developing a kinetic mechanism involves compiling a set of the elementary reactions which in turn have been derived from experiments and/or theoretical calculation.

Uncertainties in model development can be divided in *aleatory* and *epidemistic*. The first is due to probabilistic variability, it is a random and cannot be reduced; however the resulting risk can be modelled with a probability distribution function. The second is reducible since it is correlated to our limited knowledge about the system, namely poor quantification of input parameters, incomplete and/or wrong errors physical and missing chemical pathways [28, 29]. Although the methods for calculation of rate coefficient and thermodynamic data have been improved through the years, it is not possible to quantify each kinetic mechanism parameter to perfection.

To have an idea about how important it is to accurately determine rate coefficients, let us examine, as an example, one of the most experimentally investigated elementary reactions, the branching reaction $H + O_2 = O + OH$. The highest accuracy achieved for such a reaction gives an uncertainty of 2σ (standard deviation) in *k* better than 15% over the investigated temperature range of 1100-3000 K [30]. Then, for experiments where such a reaction is governing the combustion process,

e.g., LBV measurements, the sole k uncertainty is responsible for 3% of the uncertainty on the predicted LBV result [28]. Generally, although their values have been determined with greater uncertainty, rate coefficients show less impact on the uncertainty of the models. However, it has to be highlighted that whenever the modellers were forced to use kinetic homologs to estimate rate constant coefficients, as for some hydroxylated compounds, this would have resulted in a general increase of models uncertainties.

2.4.1 Local sensitivity

As previously stated, sensitivity analysis can be used to verify how a physical parameter affects the prediction of a combustion model. The logarithmic sensitivity coefficient is among the most common sensitivity measures. In this case $S_{i,j}$ is defined as the sensitivity coefficient of the i^{th} computed quantity or the model prediction y_i with respect to the j^{th} rate parameter x_j [31]:

$$S_{i,j} = \frac{logy_i - logy_i'}{logx_j - logx_j'} \tag{1.23}$$

Here x_j' is the parameter that has been "perturbed" from the reference value x_j and y_i' is the computed quantity i calculated with the modified parameter.

For small perturbations eq. (1.23) can be rewritten as:

$$S_{i,j} = \frac{\delta logy_i}{\delta logx_j} = \frac{x_j}{y_i}\frac{\delta y_i}{\delta x_j} \tag{1.24}$$

This is known as *brute force* sensitivity. In case of reaction rate sensitivity, x_j is the *A factor*, and y_i is the parameter of interest, e.g., the LBV or a species concentration.

The uncertainty parameter f is usually used to describe the uncertainty in the rate coefficient and can be defined as:

$$f(T) = Log\frac{k^0(T)}{k^{min}(T)} = Log\frac{k^{max}(T)}{k^0(T)} \tag{1.25}$$

Here k^0 is the recommended (or nominal) rate coefficient based on the available kinetic studies with its lower and upper extremes, k^{min} and k^{max}, respectively. Values outside the bounds are considered rather improbable.

2.4.2 Global sensitivity

An important tool for model with large uncertainties and non-linear models is the global sensitivity approach. Global methods are sampling-based methods attempting to cover the whole input space and they need a large number of model runs (instead of the single run needed for local sensitivity analysis). In such methods, the input parameter distributions have to be known *a priori*. Global methods are particularly useful if the sensitivity of the output changes with the values of the parameters; in fact for such cases the local sensitivity methods become inaccurate.

3 Laminar burning velocity

The velocity, relative to the unburnt gas, with which a plane, one-dimensional flame front travels along the normal to its surface, as simple as that. It was 1972 when Andrews and Bradley [32] gave the first "proper" definition of *laminar burning velocity* (LBV) perfecting the previous attempts; since then, many combustion researchers provided their own interpretation of such a definition, without however distorting its essence.

LBV is one of the key combustion characteristics of premixed flames, providing invaluable information about the exothermicity, the reactivity and the diffusivity of the fuel-oxidizer mixture [33]. Moreover, it is an intrinsic property of the combustible mixture, depending on initial temperature, pressure and mixture composition. Specifically, the influence of the initial gas temperature on LBV can be expressed via the empirical correlation

$$S_L = S_{L0} \left(T / T_0 \right)^{\alpha} \qquad (2.1)$$

Here, S_{L0} denotes the unstretched burning velocity at reference temperature T_0, while α denotes the temperature power exponent. Similarly, the initial gas pressure influence can be expressed as:

$$S_L = S_{L0} \left(P / P_0 \right)^{\beta} \qquad (2.2)$$

Here, P_0 denotes the reference pressure, while β denotes the pressure power exponent.

As for the dependence on the composition of the mixture, it is mainly related to the dependence of the flame temperature on the equivalence ratio (Φ).

Hence, LBV could be used to assess the prediction of combustion kinetic models. Moreover, the knowledge of this quantity is also helpful in understanding flame-specific phenomena like extinction, blow-out and flash-back [34]. In addition, LBV is independent from the gas flow rate, flame geometry and burner size [35], which has allowed, over the years, a proliferation of numerous methodologies suitable for its indirect determination. The word *indirect* has been used appropriately, as the LBV is not directly measurable, as a flame which propagates planar in a confined

area is influenced, among the others, by hydrodynamic instabilities, buoyancy effects, flame-wall interactions and acoustic pressure waves [36].

3.1 Experimental Techniques

The main methods employed to measure the LBV will be discussed below; in particular, the attention will be focused on the heat flux method, which was used in my experimental work, while the other methodologies will be treated in the form of a succinct excursus.

3.1.1 The heat flux method

The heat flux method (HTM) allows the stabilization of a flat premixed flame on a multi-hole burner plate under near-adiabatic conditions. Such conditions occur when the heat losses needed to stabilize the flame on the burner plate are compensated by the heat received by the inlet gases flowing through the preheated perforated burner plate. Assuming that the thermal properties, the heat fluxes at the top and bottom plate surface, as well as the burner plate temperature at the outside perimeter, are all kept constant, the radial temperature profile (measured through the use of thermocouples inserted on the bottom of the burner plate) can be expressed as follow [37, 38]:

$$T_r = T_{r_0} - \frac{q}{4\lambda h} r^2 \qquad (2.3)$$

Here r denotes the radial placement of the thermocouples, r_0 is the center of the burner plate, q is the net external heat transfer, λ is the thermal conductivity and h is the thickness of the burner plate [38].

Since Eq. (2.3) is a parabolic function, it can be rearranged as:

$$T_r = T_{r_0} + Cr^2 \qquad (2.4)$$

Where $C = -\frac{q}{4\lambda h}$ is called *parabolic coefficient*.

It is rather intuitive that the radial temperature profile T_r is strictly dependent on the fresh gas velocity, V_g . In fact, when V_g is not sufficient to reach conditions of adiabaticity, *id est*, q>0 (C<0), the temperature at the burner plate perimeter is lower than T_{r_0}, and the flame tends to be stabilized closer to the burner plate; we are in the so-called *sub-adiabatic* condition state. On the contrary, for *super-adiabatic* flames, $V_g > LBV$, namely, the flame tends to be stabilized further away from the burner

plate and the heat loss from the flame is lower than the heat gained by the fresh gases q<0 (C>0).

Since it is rather complicated to set the fresh gases flow to a condition for which C=0, LBV is usually determined using a linear interpolation procedure; however, for specific fuel + air mixture flame instabilities might occur prior to reaching adiabatic conditions. For such cases, an extrapolation procedure is necessary.

3.1.1.1 Heat flux setup

A schematic representation of the cross section of the heat flux burner, as well as of the heat flux setup, is depicted in Fig. 2 and Fig. 3, respectively, while a comprehensive description of the apparatus used for my PhD project is given below.

The burner plate consists of a perforated brass matrix (with 0.5 mm diameter holes) which has a diameter of 30 mm and a thickness of 2 mm and is secured through thermal paste to the burner head. The head is kept at a constant temperature of 368 K by a heating jacket supplied with thermostatic water; the plenum chamber is further supplied with a dedicated water heating system, which allows setting the desired initial fresh gas temperature. The measurement of the temperature distribution along the burner plate is ensured by 8 T-type thermocouples, soldered into the holes of the burner plate, which have a diameter 0.1 mm. Mass flow controllers, MFCs, (Bronkhorst High Tech.), which are remotely controlled from a personal computer via a LabVIEW script, are mounted on a mixing panel and used to set the flows of the vaporized fuel and the oxidizer, in order to set the desired equivalence ratio. In order to minimize flow fluctuations, buffer vessels are installed upstream the MFCs.

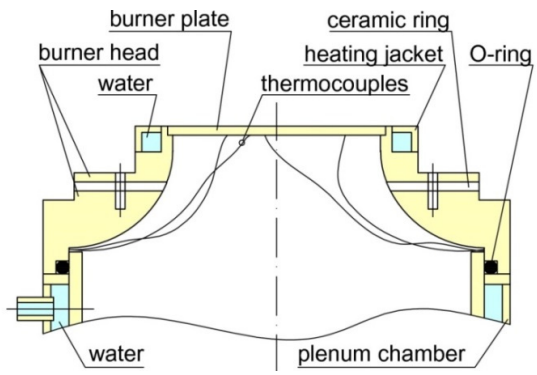

Fig.2. Cross-section of the heat flux burner, reprinted from [39].

The liquid fuel flow from the fuel reservoir, pressurized by nitrogen, is controlled through a liquid mass flow controller (Cori-Flow, Bronkhorst High-Tech) and is fed to a Controlled Evaporator Mixer (Bronkhorst High-Tech). In addition, the oxidizer flow is used as a carrier gas to facilitate fuel vaporization. A heated hose, set to the initial temperature, is used to carry the fuel + air mixture to the burner, with the aim to prevent undesirable condensation.

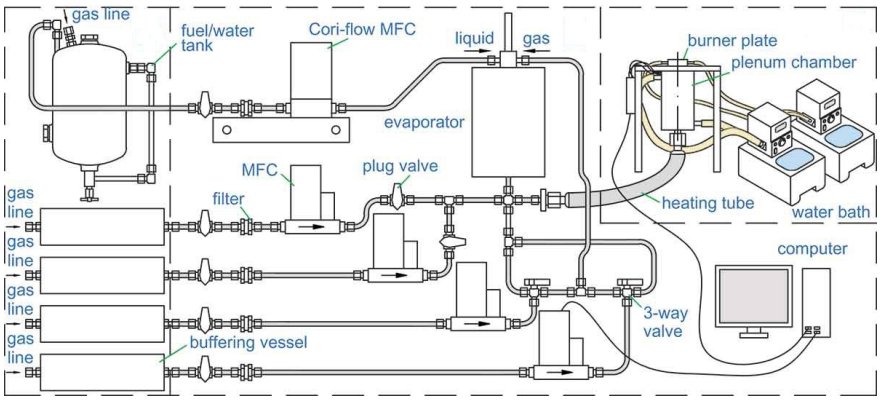

Fig.3. Schematic of the experimental setup(not in scale), reprinted from [38].

In the HTM, condensation of liquid fuels can be one of the major issues to face; such a problem become more prominent as the molecular weight of the reactant increases and at lower initial temperatures, limiting *de facto* the investigable equivalence ratio range. To assess this problem, a simple equation can be used to calculate the maximum equivalence ratio (φ) investigable for a given initial temperature T_0:

$$\Phi(T_0) < \frac{\upsilon_{O_2}}{\upsilon_F}\frac{x_F}{x_{O_2}(1-x_F)} \text{ with } x_F = \frac{P_F}{P} \qquad (2.5)$$

Here υ represent the stoichiometric coefficient, x_F is the mole fraction of the fuel, x_{O_2} is the mole fraction of the molecular oxygen in the air (0.21), and P_F the partial pressure of the fuel at the initial temperature .Prior to each experimental session, a piston meter (MesaLabs Bios DryCal Definer 220) was employed to calibrate the MFCs. The experimental uncertainty associated to the LBV measurements performed with the HFM was typically better than ± 1 cm/s. An exhaustive explanation related to the determination of the different factors contributing to the overall LBV uncertainty was provided in [38].

3.1.1.2 *Advantages and disadvantages of the HFM*

The HTM provides flat flame configurations free from stretch effects, which are well known to be one of the major sources of uncertainty in LBV determination performed with other methods, *exempli gratia*, spherical and counterflow flames [40]. In fact, when a flame is stretched, an extrapolation method has to be used in order to derive the unstretched LBV, resulting in an increase of the experimental uncertainties and so decreasing the reliability of the kinetic model validated against such experiments [37]. However, some disadvantages are also present. HFM cannot be used if the LBV of the fuel mixtures exceeds ~80 cm/s since the burner plate perforation geometry will perturb the flow of the fresh gases.

There is a limited range of initial temperatures that can be investigated, since at high temperatures the flame approaches too close to the burner leading to increased radical quenching over the burner plate [41] and the possible onset of catalytic effects of the brass plate. Moreover HFM is not suitable for performing measurements at high pressure conditions (>10 atm), since flames become unstable due to the low LBV [34].

3.1.2 Spherical flames

The most common way to measure LBV at high-pressure conditions is through the use of a closed-vessel at constant-pressure (Fig.4).

In this method, a fuel mixture is introduced into a spherical or cylindrical (less common) vessel at given φ, pressure and temperature. After being centrally ignited, a spherical flame propagates outwardly in a quiescent homogeneous combustible mixture. The ignition source is usually provided thanks to a spark discharge; however, in case of poor flammability, a laser-induced ignition can be also used.

After the deflagration, the flame surface undergoes both curvature and strain effects, which lead to modifications of its surface (*stretch effect*) [42]. The burned flame speed, S_b, is derived by evaluating the instantaneous flame radius as function of time, $S_b = \frac{dR}{dt}$. Subsequently, a linear (or non-linear) relation is used to extrapolate the zero-stretch burned flame speed S_b^0. Finally, the LBV (S_u^0) is calculated using the mass conservation equation:

$$\frac{S_b^0}{\sigma_b} = \frac{S_u^0}{\sigma_u} \qquad (2.6)$$

where σ_b and σ_u are, respectively, the densities of burnt and unburnt gases at equilibrium. For the spherical flame method, there are several sources of uncertainties that can influence the measurements, such as the accuracy of the initial reactant mixture composition, the presence of *buoyant*, *thermo-diffusive* or

hydrodynamic instabilities, *radiation heat losses* [37], as well as *ignition* and *confinement effects*. Moreover, for flame with large flame thickness, the calculation of LBV through the use of the expansion ratio determined at equilibrium has proved to be erroneous [43].

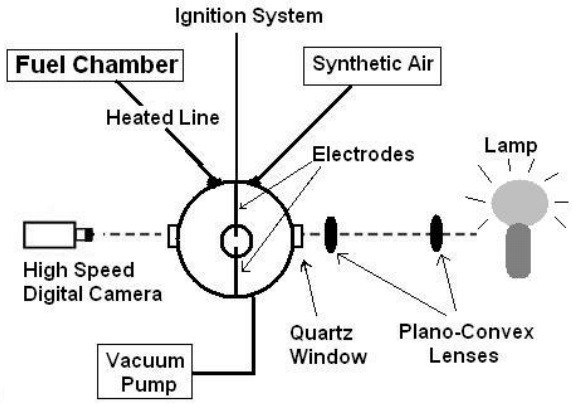

Fig.4. Schematic illustration of a typical Spherical combustion chamber setup. Reprinted from [44].

3.1.3 Stagnation flame method

In this method, a stagnation-type flow configuration is achieved when two opposite jets with identical chemical composition impinge on each other; the location where the axial velocity is equal to zero is referred as the stagnation plane (Fig. 5). For such an arrangement, there are no downstream heat losses due to the flame symmetry whereas the only loss is due to thermal radiation [37]; hence, the hydrodynamic strain is the only external effect acting on the flames [45, 46]. In case of ideal stagnation flow conditions, the flame stretch is correlated to the local radial velocity gradient, $\frac{dv}{dr}$, and then to the axial velocity gradient $\frac{du}{dx}$. In order to determine the LBV, the strain rate needs to be *extrapolated to zero-stretch*. As for spherical flames, linear or non-linear approaches can be used to extract the LBV, which affect the LBV uncertainty. Moreover, for fuels with high molecular weight, the low diffusivity leads the flame to be affected by differential diffusion, particularly at fuel-rich condition, which in turn enhances the stretch effect on the mixture reactivity and so the uncertainty in the LBV determination. Further uncertainties in stagnation flame experiments are related to the preparation of the combustible mixture in case of liquid fuel; in fact, particular attention has to be paid to the amount of vaporized fuel introduced into the combustible gaseous stream [34].

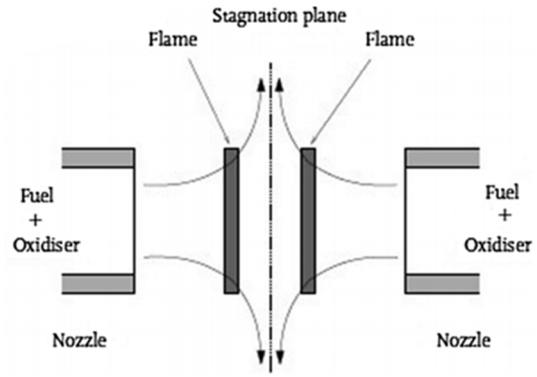

Fig.5. A schematic illustration a burner-stabilized stagnation flame, reprinted from [40].

3.1.4 Externally heated mesoscale diverging channel method

In this method, the combustible mixture flows through a channel which has a flow divergence in the transverse direction that depends on the aspect ratio (Fig.6). The fuel mixture is then ignited at the exit plane and the flame stabilized at a location where the local flame propagation velocity is equaled by the flow velocity.

In the canonical MDC configuration, the combustible mixture is affected by a positive temperature gradient due to the external preheating that heats the reactant mixture, helps in preventing thermal coupling between the gas phase and the channel walls, and also improves ignition and flame stabilization [47]. The velocity of propagating flame, *id est,* S_L, is obtained by applying the mass conservation equation:

$$\rho_0 A_0 v_0 = \rho_f A_f S_L, \tag{2.7}$$

Then, if now we use the ideal gas law in eq. (2.7):

$$S_L = v_0 \frac{A_0}{A_f} \frac{T_f}{T_0} \tag{2.8}$$

Here, subscript *0* stands for inlet and subscript *f* stands for flame.

The MDC allows investigations of LBV for a combustible mixture up to its autoignition temperature. The uncertainties related to the LBV determination performed with the MDC method are related to possible heat loss to the channel walls, boundary layer, thermal feedback, temperature gradient between reactants and solid wall and are exhaustively treated in [48].

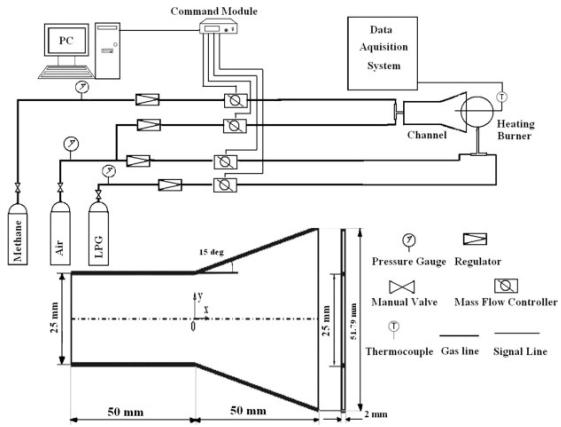

Fig.6. A schematic illustration a typical MDC, reprinted from [46].

3.2 Instabilities in burner-stabilized adiabatic flames

There are two major sources of instability, in planar premixed flames, i.e., hydrodynamic (or Landau–Darrieus) and diffusive-thermal instabilities. Hydrodynamic and diffusive-thermal instabilities, also known as *cellularities*, are responsible for the formation of cellular flame structures, which prevent to perform LBV measurements, as the flame shape deviates from the assumptions made for the LBV definition.

Hydrodynamic instabilities (Fig.7) are a consequence of the amplification of the flame front due to hydrodynamic disturbances induced by the gas expansion (change in density) resulting from the heat release during the combustion process [49].This phenomenon tends to be enhanced as the initial density and pressure (which reduce flame thickness) of the combustible mixture increase. Diffusive-thermal instabilities appear if the mass diffusivity (D) of the deficient reactant is larger than the thermal diffusivity (α), *id est*, if the Lewis number ($Le = \alpha/D$) is less than unity, which is the case for fuel-rich flames of long-chain hydrocarbons or fuel-lean hydrogen flames. However, exception may occur; in fact, for fuel-rich flames of hydrogen, diffusive-thermal instabilities occur even if $Le > 1$, due to the preferential diffusion effect caused by the reactant species [50]. For burner stabilized-flame and $Le > 1$, depending on fuel-mixture composition, initial temperature and pressure, there is a minimum stand-off distance between flame and burner plate at which the onset of cellularities occur. These instabilities can be suppressed by increasing, whenever possible, the burner plate temperature, as the flame tends to approach the burner surface, benefiting from its stabilizing effect.

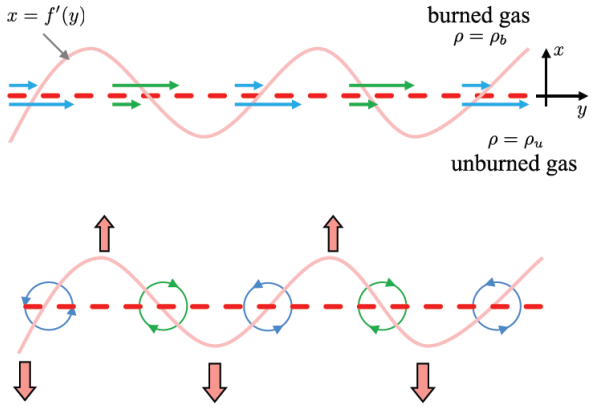

Fig. 7. Schematic representation of a planar flame affected by hydrodynamic instabilities. Reprinted from [49]. The perturbation is caused by a "jump" in the transverse velocity across the flame (up). The perturbed flame acts similarly to a flat vortex sheet of non-uniform strength with vorticity orientation (down), that causes an increase in the initial flame displacement. The expansion of the gas leads to the deflection, which in turn is responsible of an expansion or contraction of the stream-tubes, generating a pressure gradient that enhances an initial displacement of the flame [51].

4 Laser-Induced Fluorescence

Laser-Induced Fluorescence (LIF) is one of the most employed Laser-based techniques in combustion research. Using LIF it is possible to detect intermediate atom and molecular species, such as flame radicals. The LIF mechanism can be described as a two-step process: first, the targeted species in its ground state is excited by resonant absorption of laser photons to a higher energy electronic level (excited state); then, the second step involves the relaxation (de-excitation) process of the species in which a spontaneous emission of fluorescence radiation, emitted in the whole space surrounding the interaction volume, occurs. Two different approaches can be used for LIF spectroscopy investigations:

- the fluorescence spectrum, in which the laser frequency is set to a single absorption frequency of the targeted species and fluorescence spectrum, is recorded (by scanning the spectrometer wavelength);
- the excitation spectrum, which involves scanning of the laser frequency and the induced fluorescence, is detected using, for instance, an optical filter or a low resolution spectrometer. Fluorescence detection occurs at the point where the laser frequency equals the resonant absorption. Since it depends only on the laser linewidth and on the absorption line, this approach allows achieving high spectral resolution [52].

However, in LIF measurements phenomena like photoionization, predissociation and quenching may limit diagnostic capabilities of LIF. Even if photoionization can be overcome by operating on the laser power and most of the excited state do not involve predissociation, quenching effects are still a big issue that has to be treated properly. In fact, in the LIF measurements the relatively long life-time of the fluorescence (~2 ns in a flame) makes the signal very sensitive to atom/molecule collisions, which in turn can compete with the signal-generating process. This phenomenon, known as *quenching,* depends on conditions such as temperature, pressure and collision pattern and can make quantitative LIF measurements challenging. LIF measurements can be performed in the so-called *linear regime* where the *fluorescence signal* depends linearly on the *laser irradiance* (W/cm^2). However, if strong excitation is employed, the signal can be *saturated*, i.e., independent on laser irradiance and on quenching effects. Figure 8 below shows a two-level energy diagram representing the LIF principle. Here B_{12} and B_{21} are, respectively, the absorption and stimulated emissions; A_{21} is the fluorescence signal;

Q_{21} is the collisional quenching; W_{2i} and P represent, respectively photoionization and predissociation.

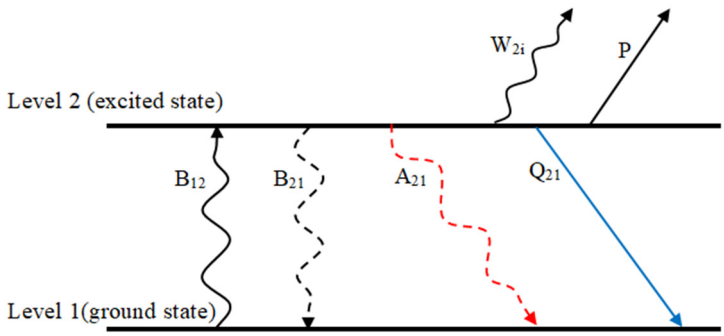

Fig.8. LIF principle.

4.1 Nitric oxide mole fraction measurements with saturated LIF

Since part of my PhD also involved nitric oxide (NO) quantitative measurements in the post-combustion zone of C_1-C_3 alcohols flames, a brief description of the method employed will be given below.

Excitation of NO in the $A^2\Sigma^+ \leftarrow X^2\Pi$ (0-0) band at wavelength 225.5 nm was ensured thanks to the employment of Nd:YAG + dye laser system. The fluorescence radiation was detected in the (1-0) vibrational band around wavelength 236 nm (Fig. 9). Measurements were made at irradiances high enough to approach saturated LIF conditions, i.e., where the signal becomes insensitive to laser irradiance. Quantitative measurements were obtained by calibration versus the NO signal measured in a lean calibration flame seeded with controlled amounts of NO. For proper conversion of signals into concentrations, the data evaluation also considered the differences in temperature and concentrations of major species in the flames, to account for differences in gas density and molecular collisions, the latter resulting in non-radiative de-excitation of NO (*quenching*) thus competing with the fluorescence emission.

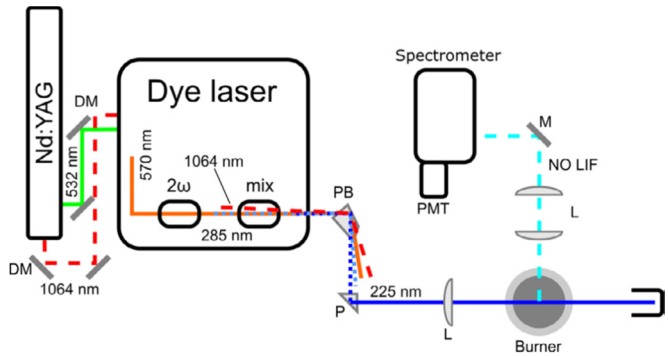

Fig. 9. Schematic representation of NO LIF setup. Reprinted from [53].

5 Detailed combustion modelling of the combustion of small oxygenated aliphatic hydrocarbons

In this chapter, selected results of the propanal and propyl alcohols combustion kinetic mechanisms from Papers I, III, and IV are presented and discussed.

5.1 Propanal

Alcohol oxidation can lead to the formation of undesirable toxic carbonyl molecules, such as saturated and unsaturated aldehydes, which can appear in non-negligible amounts in the exhaust gases of internal combustion engines; in this regard, propanal is a critical stable intermediate derived from the oxidation of 1-propanol, a promising alcohol fuel additive. While formaldehyde and acetaldehyde combustion chemistry has been extensively investigated in literature, the attention on propanal, C_2H_5CHO, oxidation kinetics is still insufficient and more fundamental studies are desirable.

The first numerical investigation of low temperature C_2H_5CHO oxidation was performed by Griffith et al. [54], on the basis of experimental data obtained in a coated Pyrex vessel. Since then, several kinetics mechanisms of propanal combustion have been developed; however, it has to be highlighted that most of propanal kinetics models proposed have been tested only against one type of experiments and therefore a development of a more general and robust chemical kinetic mechanism is needed. Hence, the major goal of this study was to develop a new detailed kinetic mechanism of C_2H_5CHO oxidation. New burning velocity measurements, obtained with the heat flux method and then free from stretch effects, along with LBV literature data [55-57], these latter performed with different methods, were used to assess the proposed model. The objective of this approach was to try to discern the nature of discrepancies that have arisen between experimental and modeled LBV that came out in [55] and to check and compare the consistency of the different burning velocity measurements by using a different experimental method. Additionally, the new kinetic model was assessed with

ignition delay times data from [58] and [59], propanal pyrolysis experiments from [60] and [61], jet stirred reactor data from [56], low-pressure flame structure [62], and, finally, compared with Veloo [56] and Polimi mechanism [63] predictions. Polimi semi-detailed (lumped) mechanism was tested in the current study, as it is well established for high temperature combustion and pyrolysis of different fuels, and assessed against burning velocities of C_0-C_4 hydrocarbons and oxygenated fuels, including propanal experimental data from [55]. Polimi was also tested in several of our recent publications [38, 64], and its modeling performance was found superior to the other kinetic mechanisms analysed.

5.1.1 Experimental results and combustion kinetic model validation

The proposed kinetic mechanism consists of 1419 reactions and 119 species and is based on the most recent Konnov mechanism provided by Fomin et al. [65], with the C_2 chemistry subset further modified by Christensen et al. [66]. In this work, the mechanism has been extended to include the chemistry of propanal oxidation. Polimi semi-detailed combustion mechanism [63] consists of over 8000 reactions and more than 250 species. In Polimi model, the kinetic scheme used to describe propanal oxidation is based on a simplified approach, i.e. C_3 radicals were accounted into a single lumped channel.

Figures 10 and 11 present the measured stretch-free laminar burning velocities for C_2H_5CHO at atmospheric pressure and at 298, 343 and 393 K. Related overall uncertainties, evaluated using procedure from Alekseev et al. [67] are represented with error bars and are commonly smaller than the symbol size of the experimental data, i.e., they are typically restricted in a range less than ±1 cm/s. When LBV measurements from this work were compared with LBV from literature, some discrepancies have been arisen and they have been attributed to different experimental problems that may arise in mixture preparation and its thermal stability during investigations employing spherical flames.

At all the tested condition, from 298 to 393K, Polimi mechanism showed closer agreement with the LBV experimental data from this study as compared to the present model. An attempt to use Veloo mechanism to simulate LBV experiments was made, however the model showed numerical stiffness that prevented its employment for the specific purpose. Further analysis has evidenced that in Veloo model $CH_2O + M = H + HCO + M$ and $CH_3 + M = CH + H_2 + M$ reactions have a reverse rate constant values exceeding collisional frequency by several orders of magnitude. This made the Veloo mechanism too stiff to be simulated and its predictions have been digitized from [56] for the temperature of 343 K. This mechanism is actually in very good agreement with the measurements of the authors [56], however, it under predict significantly the present results.

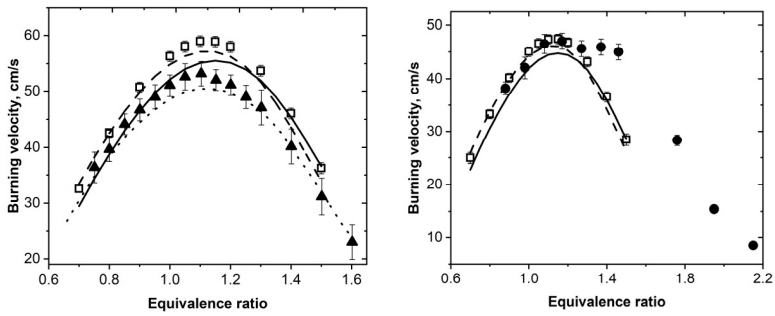

Fig.10. LBVs of C_2H_5CHO + air flames at atmospheric pressure and 298 K (left) and 343 K (right). Symbols: experiments, line: modeling. Open squares: present work; solid circles: [55]; solid triangles: [56]. Solid line: present model; dash line: prediction from Polimi mechanism [63]; dot line: prediction from Veloo mechanism [56].

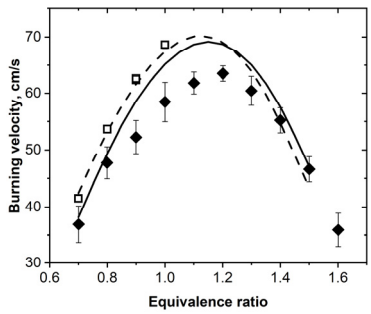

Fig.11. Laminar burning velocities of C_2H_5CHO + air flames at atmospheric pressure and 393 K. Symbols: experiments, line: modeling. Solid diamonds: [57]; open squares: present work. Solid line: present model; dash line: prediction from Polimi mechanism [63].

In attempt to find out the difference between the models behavior and to identify the most important reactions governing the combustion of C_2H_5CHO, flow rate sensitivity was also performed. Figure 12 depicts the ranked sensitivity coefficients of the C_2H_5CHO + air burning velocity with respect to the reaction rate A-factors at Φ=1.1, T=343 K and P=1 atm. Both mechanisms predictions showed that the reactivity of the system is dictated by the branching reaction $\dot{H} + O_2 \rightleftharpoons \dot{O}H + \dot{O}$ and by the reaction $CO + \dot{O}H \rightleftharpoons CO_2 + \dot{H}$. Tested models show also a common large sensitivity for the oxidation inhibiting reactions: $H\dot{C}O + \dot{H} \rightleftharpoons CO + H_2$, $\dot{C}H_3 + \dot{C}H_3 + \rightleftharpoons \dot{C}_2H_5 + \dot{H}$ and $H\dot{C}O + \dot{O}H \rightleftharpoons CO + H_2O$, as well as for the promoting reactions: $H\dot{C}O + M \rightleftharpoons H^{\cdot} + CO + M$, $\dot{H} + H\dot{O}_2 \rightleftharpoons \dot{O}H + \dot{O}H$ and $\dot{O} + H_2 \rightleftharpoons \dot{O}H + \dot{H}$. For the present model, no reactions related to the C_2H_5CHO sub-model emerged in the flow rate sensitivity analysis. Furthermore, the proposed mechanism has shown that an important contribution in promoting the flame speed is due to decomposition of ethyl radical, i.e., $\dot{C}_2H_5(+M) \rightleftharpoons C_2H_4 + \dot{H}(+M)$, and C_2H_5CHO: $C_2\dot{H}_5 + H\dot{C}O \rightleftharpoons C_2H_5CHO$ and formyl radical oxidation, i.e., $H\dot{C}O + O_2 \rightleftharpoons$

$CO + H\dot{O}_2$; a large sensitivity in reducing S_L is instead exhibited by the chain-inhibiting reactions $H_2O + M \rightleftharpoons \dot{H} + \dot{O}H + M$ and $H_2O + H_2O \rightleftharpoons \dot{H} + \dot{O}H + H_2O$ and by $\dot{H} + O_2 (+H_2O) \rightleftharpoons H\dot{O}_2(+H_2O)$. The aforementioned reactions are not pertinent for Polimi model, which instead exhibited large positive sensitivity to $\dot{C}H_3 + \dot{O}H \rightleftharpoons \dot{C}H_2S + H_2O$ and a strong negative sensitivity to $\dot{H} + \dot{O}H + M \rightleftharpoons H_2O + M$ and $\dot{H} + \dot{C}H_3(+M) \rightleftharpoons CH_4(+M)$. No fuel-specific reaction attributable to the C_2H_5CHO oxidation or pyrolysis is present and the Polimi model is sensitive only to small hydrocarbon chemistry.

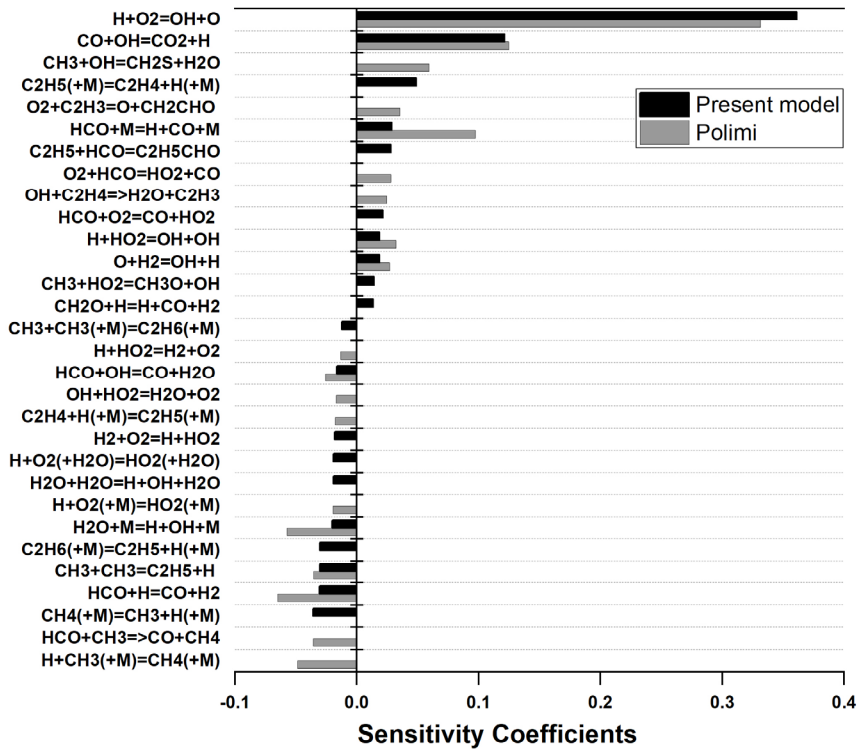

Fig.12. Flow rate sensitivity analysis of C_2H_5CHO+air laminar burning velocity at Φ=1.1, T=343 K and P=1 atm.

IDTs measurements for $C_2H_5CHO+O_2$+Ar mixtures from Akih-Kumgeh and Bergthorson [58] and Yang et al. [59] are compared with the present, Veloo and Polimi kinetic model predictions (Fig. 13). Overall, models comparison show that Veloo model has a better performance in lean and stoichiometric conditions; on the contrary, modeled IDTs from the present mechanism exhibit better performance in rich conditions. Present and Polimi models tend to sensibly overestimate mixture reactivity at high temperature regime.

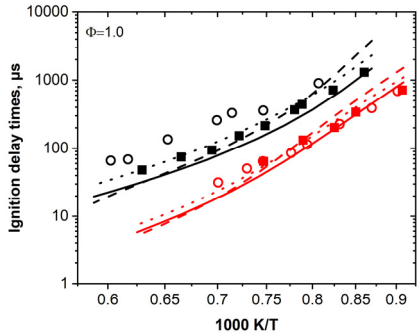

Fig.13. IDTs for C_2H_5CHO +O_2+Ar at Φ= 1.0. 1 atm (black) and 12 atm (red). Symbols: experiments, line: modeling. Solid squares: [48]; open circles: [48]. Solid lines: present model; dash lines: Polimi mechanism [53]; dot lines: Veloo mechanism [46].

In Fig. 14, models are tested against jet stirred reactor experimental data of Veloo et al. [56]. Since Polimi model [63] was developed for high temperature chemistry, no comparison is made. However, it should be noted that the updated version of the mechanism of [63], including low temperature oxidation chemistry of C_2H_5CHO has been proposed by Pelucchi et al. [68] and tested, in this study, against JSR data of [56]. Generally present model performs well in reproducing fuel reactivity at all ϕ investigated, slightly over predicting the low-temperature reactivity of the fuel. Present model shows good prediction of CO_2 and tends to underestimate H_2O concentration in high temperature region. However, such difference between model and experiments tends to decrease as ϕ increases.

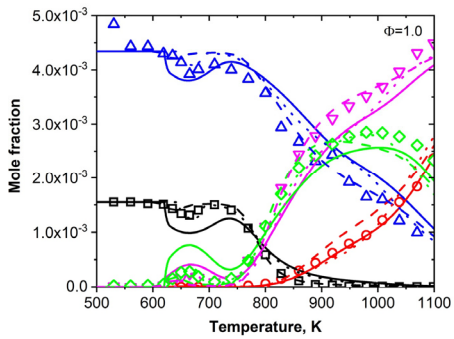

Fig.14. Mole fraction profiles of reactants and major products of in C_2H_5CHO oxidation in a JSR at Φ=0.3-2.0, P=10 atm and τ=0.7 s. Symbols: experiments [56], lines: modeling. Open squares: C_2H_5CHO; open triangles: O_2; open circles: CO_2; open down triangles: H_2O; open diamonds: CO. Solid line: present model; dash line: Pelucchi mechanism [68]; dot lines: Veloo mechanism [56].

5.1.2 Discussion on detailed kinetic mechanism of propanal

In Paper I it was observed that the presented combustion kinetic model reproduced new and literature experimental data with good agreement, in line with available models from literature. However, there is a need for more targeted experiments that can allow for further improvements of the propanal kinetic subset.

5.2 Propyl alcohols

Small aliphatic alcohols can be a valuable alternative fuels/fuel additives in SI engines, contributing to improve engine combustion efficiency and performance as their use increases antiknock index and burning velocities, if compared to traditional gasoline. Pyrolysis and oxidation kinetics of propanols has been extensively studied in the literature, including dedicated modeling works. However, from the in-depth analysis of the literature studies, it clearly emerged as the existing LBV and kinetic studies are somewhat contradictory. In virtue of the above, the aim of this study was to propose a new detailed kinetic mechanism of C_3 alcohol isomers combustion; in this regard, new LBV measurements were performed, for the first time, with the heat flux method. This method ensures robustness and reproducibility of the LBV measurements and therefore is an extremely useful tool for the model validation. Then, the proposed kinetic mechanism is also validated against LBV existing data, obtained with other different methods. In addition, another goal of this study was to try to elucidate the discrepancies that have arisen between experimental and simulated LBV that came out in previous studies [69-74] by checking and comparing the consistency of the different burning velocity measurements performed with different experimental methods. Additionally, the proposed new kinetic model was further assessed against a large literature dataset. Finally, the proposed model was compared with Sarathy et al. [75] kinetic mechanism predictions, as it showed good performance when assessed against literature data and also because it was found superior when compared with other kinetic models [76].

5.2.1 Experimental results and combustion kinetic model validation

The presented kinetic model, hierarchically structured, consists of 1787 reactions and 161 species and is based on the most recent Konnov mechanism provided by Capriolo et al. [40] with some important modification introduced by Konnov [77] i.e., the integration of the termolecular reactions associated to hydrogen oxidation, namely, $H + O_2 + R$ suggested by Klippenstein and Burke [78, 79]; furthermore, the transport properties were updated using calculations of Jasper et al. [80, 81]. In

this work, the mechanism has been extended to update and extend the chemistry of propanol isomers.

Sarathy mechanism, consisting of over 3600 reactions and more than 680 species, was tested in the current study since its C_3 alcohol isomers subsets is mainly based on the well-established mechanism [82] to which important low temperature chemical reactions have been added.

Figure 15 depicts new and available literature LBVs measurements for n-propanol and i-propanol + air flames at P=1 atm and at 343 K and 393 K. Overall uncertainties in LBVs determination related to this work were evaluated adopting Alekseev et al. [37] procedure and are represented with error bars and typically restricted in a range less than ±1 cm/s. Whenever possible, present LBV results were compared with literature data performed with different experimental method, i.e. the counterflow technique [83] and the externally heated mesoscale diverging channel (MDC) [72] at 343 K and spherical flames approach [69, 74, 84] at 393 and 423 K. For both fuels, the LBV peak lies around Φ=1.10, appearing in agreement with what was found with lower alcohol homologous; the higher values of LBVs resulting for the oxidation of n-propanol + air mixtures, are related to the higher flame temperatures (~12 K) reached for the oxidation of the primary alcohol. When compared to i-propanol, the higher reactivity of n-propanol is due to the propensity to form more reactive intermediates during its combustion process, as also stated in Veloo and Egolfopoulos study [83].

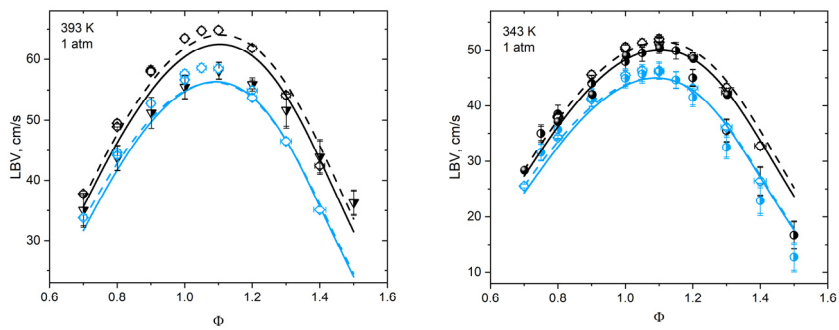

Fig.15. Laminar burning velocities of propanols + air flames. n-propanol: black; i-propanol: light blue. Symbols: experiments, line: modeling. Open diamonds: present work; half right solid circles: [83]; half right solid down triangles: [72]; solid spheres [70]. Solid line: present model; dash line: prediction from Sarathy et al. [75].

In order to check data consistency, the analysis of the temperature dependence of LBV of n-propanol + air mixture was performed at different Φ for present and literature data; the influence of the initial gas temperature was analysed in logarithmic coordinates as shown in Fig.16. An excellent congruity of the presented data is observable at all the temperatures tested and, more generally, strong methods consistency were found between the heat flux, MDC and with data from [84]

performed using spherical flames configuration, as well as with counterflow technique up to Φ=1.10, after which important deviations were encountered (8-27%). When compared with the data from [72], the present LBV measurements were found higher by approximately 11%; other important deviations were also found with measurements performed in spherical flames [69, 85]. Overall, it appears rather evident from Fig.16 that the experiments carried out with spherical flames approach [69, 74, 84] are inconsistent with each other. In this regard, further investigations are needed to comprehend the reasons of such inconsistences. As previously stated [40], one of the possible explanations might lies into the longer residence time required to perform some of the experiments using spherical flames configuration, which could result in a partial oxidation of the fuel prior to its ignition. Moreover other possible error sources in the LBV determination could be due to stretch extrapolation of the expanding flame, as well as radiation losses and compression effects dependent on the chamber size, both reducing the flame speed propagation and so the LBV values.

At all tested conditions from this study, i.e. 323 K, 343 K and 393 K, the general trend of LBV of n-propanol + air mixtures is well captured by the present and Sarathy et al. [75] models, while both slightly underestimate (~5%) the LBV of i-propanol + air mixture near stoichiometric conditions. One may note that both model behaviours are really close to each other. When compared with the literature results, the models show satisfactory performance in reproducing data from [70], [72] and [84], while discrepancies arise when compared with [69], [73], [74] studies.

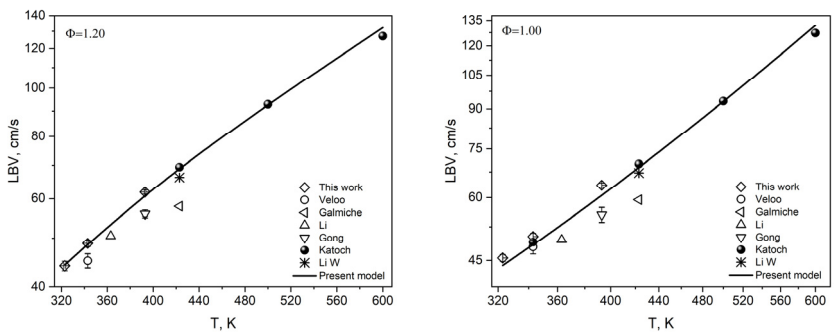

Fig.16. Laminar burning velocities of n-propanol + air as a function of inlet gas temperature at atmospheric pressure plotted in log-log scale. Symbols: experimental data, line: present model.

In Figure 17 the ignition characteristics of n- and i-propanol + O_2 + Ar mixtures from Man et al. [82] are compared with the numerical simulations performed with the present and Sarathy model. The IDTs measurements were carried out behind reflected shock waves with P=1.2, 4 and 16 atm, T=1100-1500 K, at Φ= 2.0; for both investigation the fuel concentration was set to 0.75%. Overall, both

mechanisms exhibit good performances in reproducing the experimental results. However, for n-propanol-based experiments, proposed mechanism was found superior to Sarathy model at 4 and 12 bar, while the latter model showed a closer agreement to the experiments at 1.2 bar. It has to be noted that both models sensibly overpredict the fuel mixture reactivity under rich conditions. When compared to i-propanol IDTs data, the present mechanism exhibits better performance in comparison to the Sarathy model [75] at 1.2 and 16 bar while it tends to underpredict the fuel mixture reactivity at 4 bar.

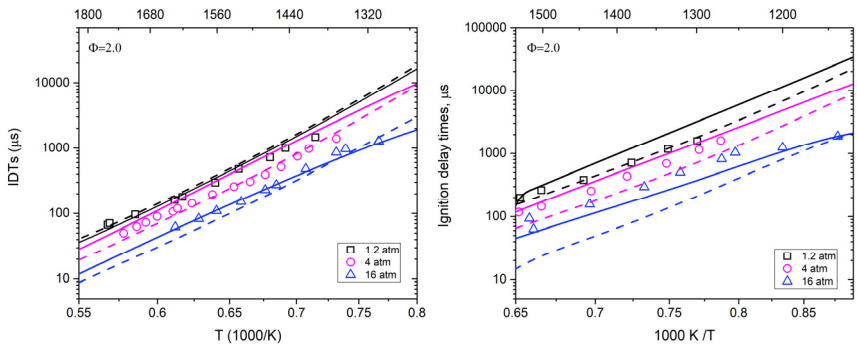

Fig.17. IDTs for n-propanol + O_2 + Ar (left) and for i-propanol + O_2 + Ar (right) from [82]. Symbols: experiments, lines: modeling. Solid lines: present model; dash lines: Sarathy mechanism [75].

To emphasize the difference between the models behaviour, brute-force sensitivity analysis of the simulated IDT's was performed with both models at T=1428 K, P=1.2 atm and at Φ=2.0 and the most sensitive reactions were ranked and depicted in Fig.18. A negative value indicates that a reaction decreases the temperature of the system, causing a longer ignition delay time. For the ignition of n-propanol, the reaction $nC_3H_7OH + H \rightleftharpoons CH_2CH_2CH_2OH + H_2$ is a reactivity-inhibiting step for the present model, while it enhances the propensity to ignite of the primary alcohol in Sarathy mechanism; such a difference is the result of the different branching ratio for the $nC_3H_7OH + H$ reaction present in the two models. For the ignition of i-propanol, the only difference between the two models is related to the reaction $CH_3COCH_3 \rightleftharpoons C_2H_6 + CO$, which inhibits the reactivity of the branched isomer and is not present in Sarathy mechanism.

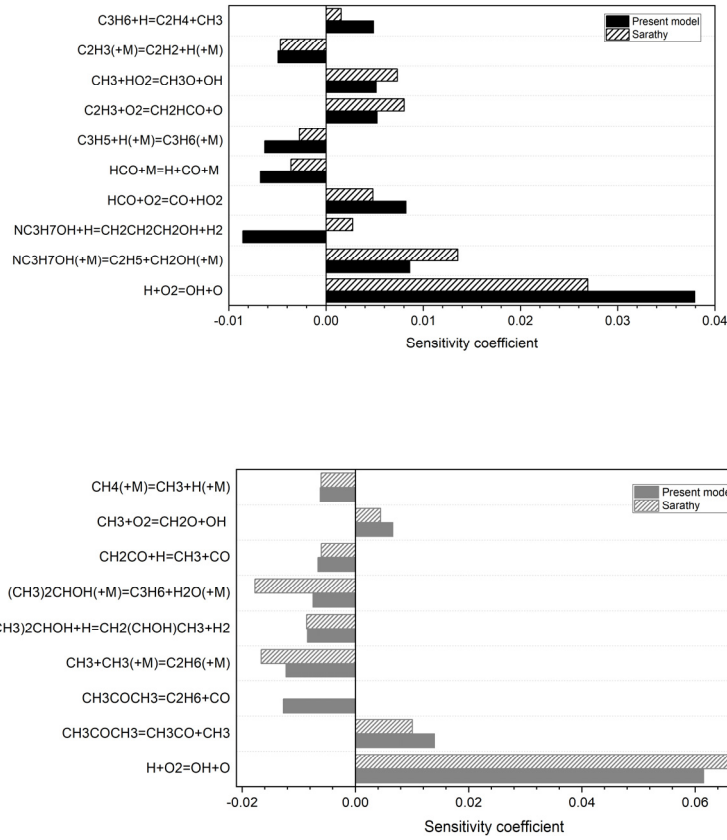

Fig.18. Sensitivity analysis of the ignition of n-propanol (black) and i-propanol (grey) at T=1428 K, P = 1.2 bar and at Φ=2.0.

The effect of temperature on n-propanol and i-propanol pyrolysis [84] is represented in Fig. 19; the experimental mole fraction profiles of the major species are compared with the present and Sarathy kinetic model predictions. Experiments were performed in a flow reactor with 3% fuel in argon, at stated flow rate of 1000 sccm. Comparison of the n-propanol experimental data with models predictions show that both models well capture n-propanol conversion and formation of some major species, such as H_2O, CH_4, CO and C_2H_4. However, they tend to underestimate the formation of some minor species profiles such as CH_3CHO and C_2H_5CHO, while C_3H_6 concentration is better represented by the present model. Regarding i-propanol pyrolysis, models show a satisfactory performance in reproducing fuel conversion and formation of major species, while some discrepancies arise with CH_3COCH_3 profile, where experimental data are overestimated and maxima shifted to higher temperature (by ~100 K).

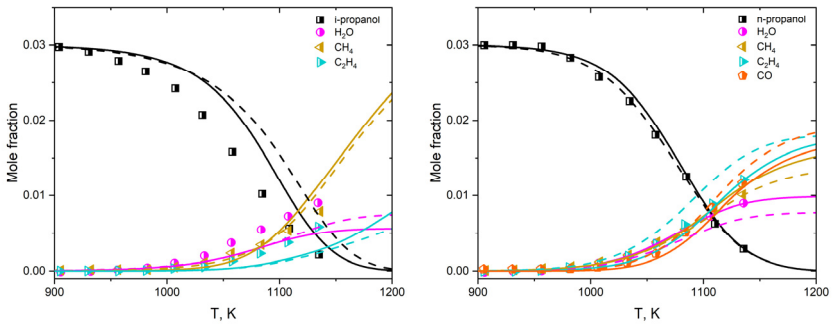

Fig.19. Mole fraction profiles of the major species for 3% n-propanol(left) and 3% i-propanol (right) pyrolysis at 1atm. Symbols: experiments [84], lines: modeling. Solid line: present model; dash line: Sarathy mechanism [74].

5.2.2 Discussion on LBV experiments and detailed kinetic mechanism of propyl alcohols

Generally, an excellent agreement was found when the new LBV measurements of n-propanol + air mixtures, carried out with the heat flux method, were compared with literature data performed using other methodologies; however, discrepancies with experiments performed in spherical flames have been arisen and, more generally, spherical flame measurements were found inconsistent with each other. Once again, as in Paper I, such differences were attributed to the possible oxidative phenomena occurring to the combustible mixture prior its ignition.

The detailed kinetic model for propyl alcohol combustion presented in Paper III successfully reproduce new and literature data; particularly, the newly developed model show a closer fidelity in representing IDTs data obtained at high pressure conditions.

5.3 Nitric oxide formation in premixed C_3 alcohols flames

Nitric oxide (NO) is the most abundant species of NO_x emissions [86]. In this regard, improving the understanding of the combustion chemistry of NO formation in alcohol + air flames via accurate measurements and subsequent development of appropriate kinetic models is a critical step for the design of proper clean combustion engines. Only few dedicated studies on NO formation and consumption from propyl alcohols fuels are available in literature [87-91]. Therefore, the aim of this Paper IV was to present new accurate experimental data on NO formation in C_3

alcohols + air flames. In this regard, flames were stabilized on the heat flux burner and quantitative NO concentrations were measured in the post-combustion zone by means of saturated laser-induced fluorescence (LIF).

In addition, new laminar burning velocity (LBV) data of propyl alcohols + air mixtures obtained with the heat flux method were also performed. The HFM approach permits an accurate LBV determination which in turn enables a proper evaluation of the chemical time scales of the fuel mixtures, and then allows a direct comparison of NO formed via the thermal route with kinetic predictions, contrary to the methods employed in previous studies, [88, 90, 91].

5.3.1 Experimental results and kinetic model validation

The heat flux method and the LIF technique were employed to measure the NO formation in propyl alcohols + air flames at 1 atm, for equivalence ratios ϕ = 0.7-1.4 and at height above the burner (HAB) of 10 mm (post-flame region). The unburned mixture temperature was set to 323 K for both fuel mixtures. The new combustion mechanism presented is hierarchically structured, consists of 203 species and 2295 reactions and is based on the recently proposed propanol mechanism provided by Capriolo et al. [92] in which important modifications introduced by Konnov [93] were implemented, namely the integration of the termolecular reactions associated to hydrogen oxidation, namely, $H + O_2 + R$ suggested by Klippenstein and Burke [78, 79]; furthermore, transport properties were updated using calculations of Jasper et al. [80, 81]. The implemented NO_x chemistry is based on the Konnov subset [94], to which several modifications and updates have been introduced. Specifically, reactions pertinent to N-O chemistry (chemistry of NO_x) have been revisited by Volkov et al. [95]. Moreover, the rate constant of the key thermal-NO reaction $N_2 + O \rightleftharpoons NO + N$ was also updated adopting the expression of Abian et al. [96]. New thermodynamic data [97] were implemented for NH, NH_2, NNH, HNO, HONO, HNOH, H_2NO, NH_2OH, NO_3, HNO_3, N_2O_4, N_2H_2, and N_2H_3.

The other combustion mechanisms used for kinetic assessments include the Bohon et al. [91] and the Polimi [98-101] mechanisms.

Figure 20 below depicts measured and simulated concentrations of NO at HAB=10 mm (post-combustion zone), for propyl alcohols + air mixtures. The experimental accuracy related to the NO quantification procedure is ±8.7%; further details regarding its evaluation method are available in our recent work [53]. In addition and simultaneously with NO quantification, LBVs measurements for C_3 alcohols were performed. At the investigated conditions and for both fuel + air mixtures, the peak in NO formation was located at stoichiometric condition where the maximum flame temperature is reached and the thermal-NO contribution becomes more prominent. Particularly, a comparative analysis performed with the proposed kinetic

model showed that, at stoichiometric conditions, the flame temperature for n-propanol + air mixture is ~12 K higher than for its structural isomer and this, in turn, corroborate the higher value of the thermal-NO concentration found for n-propanol (~10%), see Fig. 20.

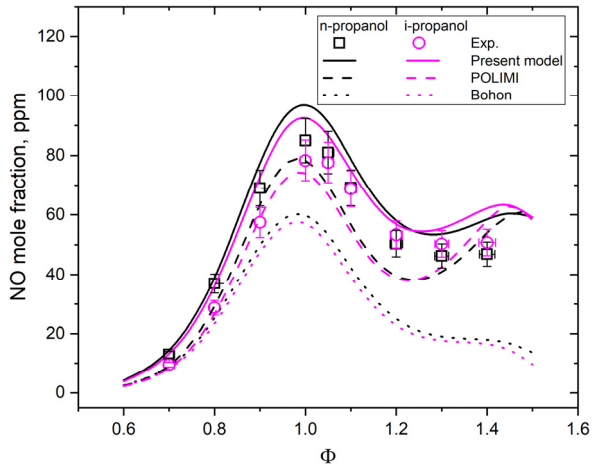

Fig.20. Experimental and simulated NO concentrations in propyl alcohols + air flames at HAB=10 mm.

However, due to the propensity to form stable intermediates, i-propanol showed lower LBV values than n-propanol (by ~8%), and so the longer residence time might have mitigated the difference in NO formation between the two isomers. In fuel-rich conditions, the non-negligible NO concentration is directly ascribable to the presence of the CH radical, playing a key role in Fenimore's prompt-NO formation [22, 102, 103]. Moreover, one may note that from Φ=1.2, the NO production in i-propanol flames become higher than the one observed in n-propanol flames; this interesting aspect will be discussed following the comparative analysis of the kinetic models. One may note that, at the investigated conditions, NO concentrations in both alcohol isomer flames were similar and the differences are within overlapping error bars; however, such errors are systematic and therefore they do influence each measurement in the same way, allowing the discernment of the different NO formation patterns and trends in the propyl alcohols flames.

At the tested conditions, the overall NO formation profiles from propanols + air flames are captured by the present model, while the Bohon mechanism fails in representing the experimental trend, especially at fuel-rich conditions. One may note that, as also previously observed, the Bohon model performances notably underestimate experimental results [91].

Figure 21 depict LBV measurements for C_3 alcohol isomers performed, as mentioned, during the NO concentration measurements. All tested models

accurately predict the experimental data, therefore the major differences in the predicted thermal-NO are attributable only to the different NO_x subsets.

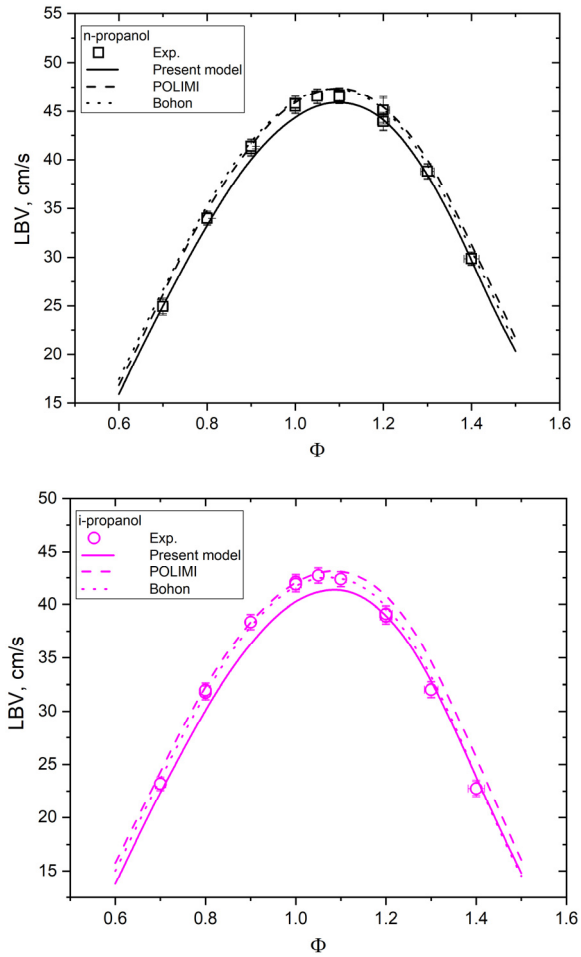

Fig.21. Laminar burning velocities of n-propanols + air mixtures and of i-propanols + air mixtures at atmospheric pressure and 323 K. Symbols: experiments, line: modeling.

Sensitivity analysis allows to identify the most important reactions governing the NO formation/consumption, as well as to highlight the difference among model behaviors. Figures 22 and 23 depict the sensitivity coefficients, simulated with the present model, for NO concentration in the propanols flame at HAB=10 mm, at Φ=1.0 and Φ=1.3. For both fuels, mechanisms predictions showed that NO formation at stoichiometric conditions is dictated by the Zel'dovich reaction $N + NO \rightleftharpoons N_2 + O$ and by the branching reaction $H + O_2 \rightleftharpoons OH + O$. The present

model also shows a large positive sensitivity to formation of NO via the NNH route, i.e., $NNH + O \rightleftharpoons NH + NO$.

At Φ=1.30 the most important reactions promoting NO formation are related to the prompt-NO route as well as to the key radicals CH and triplet methylene (CH_2). Particularly, present model considers that the reaction $CH + N_2 \rightleftharpoons NCN + H$ governs the initial step in prompt-NO formation. Moreover, the model shows sensitivity, as inhibitory reaction steps, to the scission of the hyperconjugated C_α-H bond by the H atom of the two alcohol isomers, i.e., $NC_3H_7OH + H \rightleftharpoons CH_3CH_2CHOH + H_2$ and $(CH_3)_2CHOH + H \rightleftharpoons (CH_3)_2COH + H_2$.

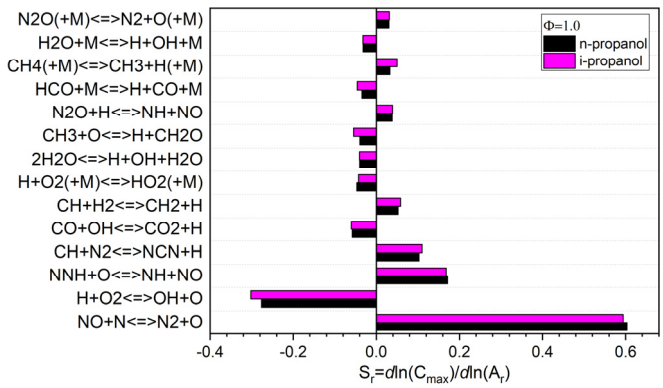

Fig.22. Present model sensitivity analysis for the NO concentrations in propanols flames at Φ=1.0 and HAB=10 mm.

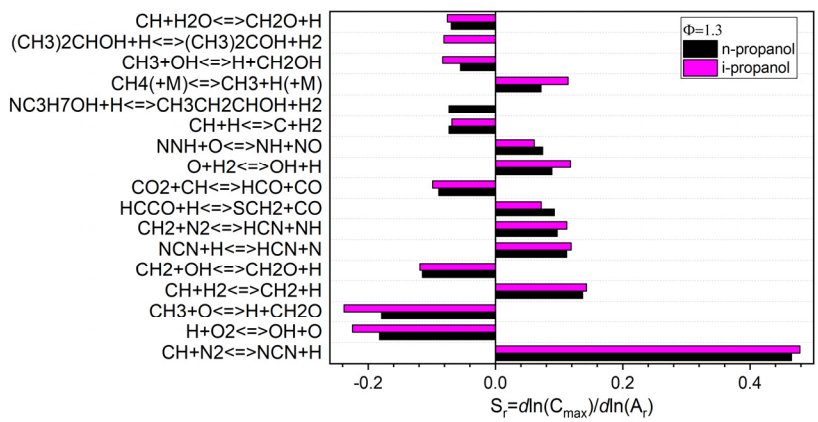

Fig.23. Present model sensitivity analysis for the NO concentrations in propanols flames at Φ=1.3 and HAB=10 mm.

With the purpose to elucidate the peculiarity of the higher NO concentration in fuel-rich i-propanol flames, rate of production analysis (ROP) of NO was performed for both C_3 alcohol fuels with the current model, at Φ=1.3 (Fig. 24) and at the maximum

value of CH mole fraction. It was found, for both isomers, that the most important reactions involved a competition between the reburning and formation mechanisms. Specifically, as already highlighted in [88], the NO-HCN reburning sub-mechanism plays a fundamental role, contributing to NO depletion by means the reaction $HCCO + NO \rightleftharpoons HCNO + CO$. Subsequently a conspicuous amount of isocyanic acid is reconverted to NO via the reaction $HCNO + OH \rightleftharpoons NO + CH_2O$. Moreover, other important reactions involved in NO consumption and formation are, respectively, $CH + NO \rightleftharpoons HCN + O$ and $N + OH \rightleftharpoons NO + H$. In particular, the effects of the reburning and the formation competition lead to a general slowdown of NO formation through the prompt-NO pathway, more pronounced in n-propanol flames in which the amount of HCCO produced was found higher by approximately 10%.

Specifically, the oxidative process of the primary alcohol leads to the formation of propanal, CH_3CH_2CHO and subsequently, via unimolecular dissociation, to ethyl (C_2H_5) and formyl (HCO) radicals, favoring the HCCO formation process via the ethylene (C_2H_4) and the acetylene (C_2H_2) routes. On the contrary, the i-propanol oxidation pathway involves formation of the acetyl radical (CH_3CO) via unimolecular dissociation of acetone CH_3COCH_3, which in turn dissociates to produce CH_3 and carbon monoxide (CO), disfavoring the formation of C_2H_4 and C_2H_2 leading to the HCCO production.

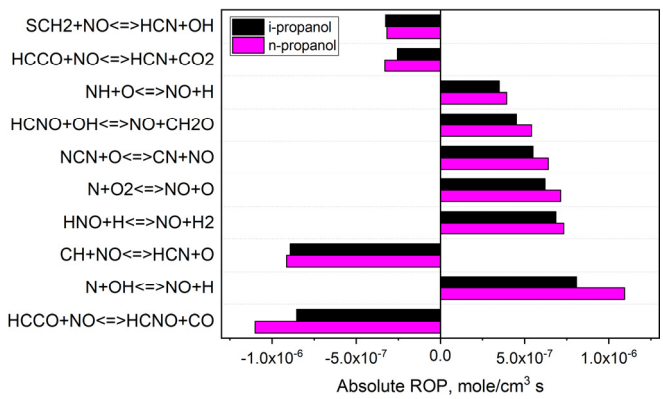

Fig.24. ROP of NO at the maximum value of CH and at Φ=1.3 for propyl alcohols + air flames.

5.3.2 Experiments and modeling discussions

Higher NO formation in the thermal region was found in n-propanol flames due to its intrinsic higher reactivity; on the contrary, in the fuel-rich zone the major NO production was detected in i-propanol flames. ROP analysis performed at Φ=1.3 with the proposed model revealed that prompt-NO formation was scaled by the NO-HCN reburning ruote. Such an effect was more pronounced in n-propanol flames, since HCCO production was favored in the oxidative process of the primary alcohol. Overall, models comparison revealed that, as expected, the distincted simulated results in the thermal and prompt regions are principally attributable, respectively, to the key Zel´dovich and Fenimore reactions employed. The Bohon and POLIMI models did not represent experimental data satisfactorily, while the present model reproduced the kinetics of NO formation with the closest fidelity. To summarize, all the tested models, albeit in different ways, need to be improved to better reproduce NO production in propyl alcohols flames, restating the importance of the provided experimental data to further ameliorate the knowledge about kinetics of NO formation.

Acknowledgments

First of all I would like to thank my supervisor Prof. *Alexander Konnov* to have given me the chance to get a PhD. Alexander, I made you laugh four or five times during my PhD years. I consider it a great personal success.

I'd like to thank my supervisor Dr. *Christian Brackmann*; even though you were constantly busy, you were always available to answer to my all my questions, I really appreciate it.

A special thanks to *Vladimir Alekseev*. I literally bombarded you with tons of questions during my first PhD year, yet you've always been so kind to reply, and after that…you left. Jokes aside, you helped me out even later, so thank you very much.

Torsten, *Torsten*! A superchill and superkind German guy! I really learned so much from you when we shared the office. I really enjoyed our politically incorrect debates and your being "not so German". Thank you for everything.

Marco, my "corregionale". Luckily *Alexander* hired you and I finally had the chance to talk about (and watch) football, drinking beers (for me just one, as usual), complaining about Italian politics etc. You have been really supportive through these years, thank you very much.

Alexios, thank you very much to you and *Panagiota* for being so helpful, especially at the very beginning when I knew nothing about Swedish laws & traditions. You are very good guys with big hearts.

Arman, do not make me laugh before I thank you, you were so funny and always ready to hear my complaining but above all you were really impressed about my gym devotion. Right now, I am pretty sure you figured it out why...

A big thank you to *Marcus*, I remember I had just started my PhD and I was invited to your place for the *sommarfika*, what a nice welcome! That day Dina told me that I was about the get a lot of *fika* during my PhD studies, I could not ask anything better, kanon!

I also like to thank *Cecilia*, *Manu*, *Sven-Inge, Frederik, Saeed* and *Minna* for the nice and funny talks we had and all the other division members, I will always have good memories about all of you guys.

Dad, *mum*, you never question any decision I took in my life, you always believed in me and in what I was capable to do. I actually love you guys more than words can say.

Nicole, you flooded my life with an ocean of sparkling energy and emotions. I love you, my nerdy wife. Thanks for being part of my life.

And the last but the most important one is you *Katherine E.*, you are literally the centre of my world, the biggest part of my heart, how would I do without your wonderful smiles?

References

[1] F.N. Egolfopoulos, N. Hansen, Y. Ju, K. Kohse-Höinghaus, C.K. Law, F. Qi, Advances and challenges in laminar flame experiments and implications for combustion chemistry, Prog. Energy Combust. Sci. 43 (2014) 36-67.

[2] H. Pitsch. A C ++ Computer Program for 0D Combustion and 1D Laminar Flame Calcula tions. http://www.itv.rwth-aachen.de/downloads/ flamemaster/, 1990.

[3] D.G. Goodwin, H.K. Moffat, R.L. Speth, Cantera: An object-oriented software toolkit for chemical kinetics, thermodynamics, and transport processes, http://www.cantera.org, Version 2.2.0 (2015).

[4] A. Cuoci, A. Frassoldati, T. Faravelli, E. Ranzi, Formation of soot and nitrogen oxides in unsteady counterflow diffusion flames, Combust. Flame 156 (2009) 2010–22.

[5] A. Cuoci, A. Frassoldati, T. Faravelli, E. Ranzi, A computational tool for the detailed kinetic modeling of laminar flames: Application to C_2H_4/CH_4 coflow flames, Combust. Flame 160 (2013) 870–86.

[6] ANSYS CHEMKIN 17.0 (15151). 2016. ANSYS Reaction Design, San Diego.

[7] LOGEresearch v 1.10 (LOGE AB) –www.logesoft.com/loge-software/.

[8] http://www.rotexo.com/index.php/en/.

[9] http://www.kintechlab.com/products/ chemical-workbench/.

[10] H. Curran, Developing detailed chemical kinetic mechanisms for fuel combustion, Proc. Combust. Inst., 37 (2019) 57-81.

[11] P.A. Willems, G.G. Froment, Kinetic modeling of the thermal cracking of hydrocarbons. 1. Calculation of frequency factor, Ind. Eng. Chem. Res. 27 (1988) 1959-66.

[12] C.J. Huang, Arrhenius Activation Energy Effect on Free Convection About a Permeable Horizontal Cylinder in A + B Porous Media, Transp. Porous Med. 128 (2019) 723–740. https://doi.org/10.1007/s11242-019-01267-1

[13] F.A. Lindermann, S. Arrhenius, I. Langmuir, N.R. Dhar, J. Perrin, W.C. McC. Lewis, Discussion on the “radiation theory of chemical action”, Trans. Faraday Soc. 17 (1922) 598-606.

[14] H.H. Carstensen, A.M. Dean, The kinetics of pressure-dependent reactions, R.W. Carr (Ed.), Modeling of chemical reactions, Elsevier, Amsterdam (2007) 105-87.

[15] R.G. Gilbert, K. Luther, J. Troe, Theory of Thermal Unimolecular Reactions in the Fall-off Range. II. Weak Collision Rate Constants, Berichte der Bunsengesellschaft für physikalische Chemie 87(2) (1983) 169-77.

[16] R.W. Carr, Modeling of Chemical Reactions, Elsevier B.V., Amsterdam (2007), 104.

[17] J. Zádor, C.A. Taatjes, R. X. Fernandes, Kinetics of elementary reactions in low temperature autoignition chemistry, Prog. Energy Combust. Sci. 37(4) (2011) 371-421.

[18] E. Blurock, F. Battin-Leclerc Modeling Combustion with Detailed Kinetic Mechanisms. In: F. Battin-Leclerc, J. Simmie , E. Blurock, Cleaner Combustion. Green Energy and Technology. Springer, London (2013).

[19] S.M. Sarathy, C.K. Westbrook, M. Mehl, W.J. Pitz, C. Togbe, P. Dagaut, H. Wang, M.A. Oehlschlaeger, U. Niemann, K. Seshadri, P.S. Veloo, C. Ji, F.N. Egolfopoulos, T.Lu, Comprehensive chemical kinetic modeling of the oxidation of 2-methylalkanes from C_7 to C_{20}. Combust Flame 158 (2011) 2338–57.

[20] C.K. Law, Combustion physics, Cambridge University Press, New York (2006).

[21] D.L. Baulch, C.T. Bowman, C.J. Cobos, R.A. Cox, T. Just, J.A. Kerr, M.J. Pilling, D. Stocker, J. Troe, W. Tsang, R.W. Walker, J. Warnatz, Evaluated kinetic data for combustion modeling: supplement II, J. Phys. Chem. Ref. Data 34(2005) 757–1397.

[22] P. Glarborg, J.A. Miller, B. Ruscic, S.J. Klippenstein, Modeling nitrogen chemistry in combustion, Prog. Energy Combust. Sci., 67 (2018) 31-68.

[23] C.P. Fenimore, Formation of Nitric Oxide in Premixed Hydrocarbon Flames, Proc. Combust. Inst., 13 (1971) 373-80.

[24] M.R. Roomina, R.W. Bilger, Conditional moment closure (CMC) predictions of a turbulent methane-air jet flame, Combust. Flame, 125 (2001) 1176-95.

[25] S. J. Klippenstein, M. Pfeifle, A. W. Jasper and P. Glarborg, Theory and modeling of relevance to prompt-NO formation at high pressure, Combustion and Flame, 195 (2018) 3–17.

[26] L. Cui, K. Morokuma, J.M. Bowman, S.J. Klippenstein, The spin-forbidden reaction $CH + N_2 \rightarrow HCN + N$ revisited. II. Nonadiabatic transition state theory and application, J. Chem. Phys. 110 (1999) 9469-82.

[27] L.V. Moskaleva, M.C. Lin, The spin-conserved reaction $CH + N_2 \rightarrow H + NCN$: A major pathway to prompt NO studied by quantum/statistical theory calculations and kinetic modeling of rate constant, Proc. Combust. Inst. 28 (2000) 2393-401.

[28] H. Wang, D.A. Sheen, Combustion kinetic model uncertainty quantification, propagation and minimization, Prog. Energy Combust. Sci., 47(2015) 1-31.

[29] Tomlin A.S., Turányi T. (2013) Investigation and Improvement of Reaction Mechanisms Using Sensitivity Analysis and Optimization. In: Battin-Leclerc F., Simmie J., Blurock E. (eds) Cleaner Combustion. Green Energy and Technology. Springer, London.

[30] Z. Hong, D. Davidson, E. Barbour, R. Hanson, A new shock tube study of the $H+O_2 \rightarrow OH+O$ reaction rate using tunable diode laser absorption of H_2O near 2.5 μm, Proc. Combust. Inst. 33 (2011) 309-16

[31] W. Gardiner Jr, The pC, pR, pP, pM, and pS method for formulating the results of computer modeling studies of chemical reactions, J. Phys. Chem. 81 (1977) 2367-71.

[32] D.E. Andrews, D. Bradley, Determination of burning velocities: A critical review, Combust. Flame 18(1) (1972) 133-53.

[33] C.K. Law, Combustion Physics, Cambridge University Press; 2010.

[34] A.A. Konnov, A. Mohammad, V.R. Kishore, N.I. Kim, C. Prathap, S. Kumar, A comprehensive review of measurements and data analysis of laminar burning velocities for various fuel + air mixtures, Prog. Energy Combust. Sci., 68 (2018) 197-267.

[35] L. Pizzuti, C.A. Martins, P.T. Lacava, Laminar burning velocity and flammability limits in biogas: A literature review, Renew. Sust. Energ. Rev. 63(2016) 856-865.

[36] B. Lewis, G. von Elbe, Determination of the speed of flames and temperature distribution in a spherical bomb from time-pressure explosion records. J. Chem. Phys. 2(5) (1934) 283-90.

[37] K.J. Bosschaart, Analysis of the Heat Flux Method for Measuring Burning Velocities, PhD Thesis, Technische Universiteit Eindhoven, Eindhoven, 2002.

[38] V.A. Alekseev, J.D. Naucler, M. Christensen, E.J.K. Nilsson, E.N. Volkov, L.P.H. de Goey, A.A. Konnov, Experimental uncertainties of the heat flux method for measuring burning velocities, Combust. Sci. Technol. 188 (2016) 853–94.

[39] V.A Alekseev, M. Christensen, E. Berrocal, E.J.K. Nilsson, A.A. Konnov, Laminar premixed flat non-stretched lean flames of hydrogen in air, Combust. Flame 162 (2015) 4063–74.

[40] G. Capriolo, V.A. Alekseev, A.A. Konnov, An experimental and kinetic study of propanal oxidation, Combust. Flame 197 (2018) 11-21.

[41] R.T.E Hermanns, Laminar burning velocities of methane-hydrogen air mixtures, Eindhoven University of Technology; 2007.

[42] N. Lamoureux, N. Djebaïli-Chaumeix, C.-E. Paillard, Laminar flame velocity determination for H_2–air–He–CO_2 mixtures using the spherical bomb method, Exp. Therm. Fluid Sci. 27(4) (2003) 385-93.

[43] J.D. Naucler, E.J. Nilsson, A.A. Konnov, Laminar burning velocity of nitromethane + air flames: A comparison of flat and spherical flames. Combust. Flame 162(10) (2015) 3803–9.

[44] Coudour, K. Chetehouna, L. Courty, F. Lemée, C. Mounaïm-Rousselle, F. Halter, Combustion characteristics of two biogenic volatile organic compounds: l-fenchone and 3-hexen-1-ol, Combust. Sci. Technol., 186 (2014) 1–11.

[45] A.W. Forman, Combustion theory. 2nd ed. Princeton, New Jersey: The Benjamin/Cummings Publishing Company; 1984.

[46] F.A. Williams, Combustion theory, Redwood city, CA: Addison-Wesley; 1985.

[47] M. Akram, S. Kumar, Experimental studies on dynamics of methane–air premixed flame in meso-scale diverging channels, Combust. Flame 158(5) (2011) 915-24.

[48] M. Akram, S. Kumar, Measurement of laminar burning velocity of liquified petroleum gas air mixtures at elevated temperatures, Energy Fuels 26 (2012) 3267-74.

[49] M. Matalon, The Darrieus-Landau of premixed flames, Fluid Dyn. Res. 50 (2018) 051412.

[50] A.A. Konnov, I.V. Dyakov, Measurement of propagation speeds in adiabatic cellular premixed flames of CH_4+O_2+CO_2, Exp. Therm. Fluid Sci., 29 (8) (2005) 901-7.

[51] M. Matalon, Flame dynamics, Proc. Combust. Inst. 32(1) (2009) 57-82.

[52] J. Amorim, G. Baravian, J. Jolly, Laser-induced resonance fluorescence as a diagnostic technique in non-thermal equilibrium plasmas, J. Phys. D: Appl. Phys. 33 (2000) R51.

[53] C. Brackmann, T. Methling, M. Lubrano Lavadera, G. Capriolo, A.A Konnov, Experimental and modeling study of nitric oxide formation in premixed methanol + air flames, Combust. Flame 213 (2020) 322–30.

[54] J.F. Griffiths, G. Skirrow, C.F.H. Tipper, A reappraisal of low temperature aldehyde oxidation using numerical analysis, Combust. Flame 12 (1968) 360–6.

[55] A.A. Burluka, M. Harker, H. Osman, C.G.W. Sheppard, A.A. Konnov, Laminar burning velocities of three C_3H_6O isomers at atmospheric pressure, Fuel 89 (2010) 2864–72.

[56] P.S. Veloo, P. Dagaut, C. Togbé, G. Dayma, S.M. Sarathy, C.K. Westbrook, F.N. Egolfopoulos, Jet-stirred reactor and flame studies of propanal oxidation, Proc. Combust. Inst. 34 (1) (2013) 599-606.

[57] J. Gong, S. Zhang, Y. Cheng, Z. Huang, C. Tang, J. Zhang, A comparative study of n-propanol, propanal, acetone, and propane combustion in laminar flames, Proc. Combust. Inst. 35 (2015) 795–801.

[58] B. Akih-Kumgeh, J.M. Bergthorson, Ignition of C_3 oxygenated hydrocarbons and chemical kinetic modeling of propanal oxidation, Combust. Flame 158 (2011) 1877–1889.

[59] K. Yang, C. Zhan, X. Man, L. Guan, Z. Huang, C. Tang, Shock tube study on propanal ignition and the comparison to propane, n-propanol and i-propanol, Energy Fuels 30 (2016) 717−724.

[60] A. Lifshitz, C. Tamburu, A. Suslensky, Decomposition of Propanal at Elevated Temperatures. Experimental and Modeling Study, J. Phys. Chem. 94 (1990) 2912–66.

[61] M. Pelucchi, K.P. Somers, K. Yasunaga, U. Burke, A. Frassoldati, E. Ranzi, H.J. Curran, T. Faravelli, An experimental and kinetic modeling study of the pyrolysis and oxidation of n-C_3–C_5 aldehydes in shock tubes, Combust. Flame 162 (2015) 265-86.

[62] V. Dias, J. Vandooren, H. Jeanmart, Experimental and Modeling Study of Propanal/H_2/O_2/Ar Flames at Low Pressure, Combust. Sci. Technol. 188 (4–5) (2016) 556-70.

[63] E. Ranzi, A. Frassoldati, R. Grana, A. Cuoci, T. Faravelli, A.P. Kelley, C.K. Law, Hierachical and comparative kinetic modeling of laminar flame speeds of hydrocarbon and oxygenated fuels, Prog. Energy Combust. Sci. 38 (2012) 468-501.

[64] V.A Alekseev, M. Christensen, E. Berrocal, E.J.K. Nilsson, A.A. Konnov, Laminar premixed flat non-stretched lean flames of hydrogen in air, Combust. Flame 162 (2015) 4063-74.

[65] J. Mendes, C.W. Zhou, H.J. Curran, Theoretical Chemical Kinetic Study of the H-Atom Abstraction Reactions from Aldehydes and Acids by Ḣ Atoms and ȮH, $H\dot{O}_2$, and $\dot{C}H_3$ Radicals, J. Phys. Chem. A 118 (51) (2014) 12089–104.

[66] M. Christensen, A. A. Konnov, Laminar burning velocity of diacetyl + air flames. Further assessment of combustion chemistry of ketene, Combust. Flame 178 (2017) 97-110.

[67] A. Fomin, T. Zavlev, V.A. Alekseev, I. Rahinov, S. Cheskis, A.A. Konnov, Experimental and modelling study of $^1CH_2$ in premixed very rich methane flames, Combust. Flame 171 (2016) 198-210.

[68] M. Pelucchi, E. Ranzi, A. Frassoldati, T. Faravelli, Alkyl radicals rule the low temperature oxidation of long chain aldehydes, Proc. Combust. Inst. 36 (2017) 393–401.

[69] B. Galmiche, C. Togbé, P. Dagaut, F. Halter, F. Foucher, Experimental and Detailed Kinetic Modeling Study of the Oxidation of 1-Propanol in a Pressurized Jet-Stirred Reactor (JSR) and a Combustion Bomb, Energy Fuels 25 (5) (2011) 2013–21.

[70] C. Togbé, P. Dagaut, F. Halter, F. Foucher, 2-Propanol Oxidation in a Pressurized Jet-Stirred Reactor (JSR) and Combustion Bomb: Experimental and Detailed Kinetic Modeling Study, Energy Fuels 25 (2011) 676-83.

[71] B. Akih-Kumgeh, J.M. Bergthorson, Ignition of C_3 oxygenated hydrocarbons and chemical kinetic modeling of propanal oxidation, Combust. Flame 158 (2011) 1877–89.

[72] A. Katoch, A. Chauhan, S. Kumar, Laminar burning velocity of n-propanol and air mixtures at elevated mixture temperatures, Energy Fuels 32 (2018) 6363−70.

[73] J. Beeckmann, L. Cai, H. Pitsch, Experimental investigation of the laminar burning velocities of methanol, ethanol, n-propanol, and n-butanol at high pressure, Fuel 117 (2014) 340–50.

[74] J. Gong, S. Zhang, Y. Cheng, Z. Huang, C. Tang, J. Zhang, A comparative study of n-propanol, propanal, acetone, and propane combustion in laminar flames, Proc. Combust. Inst. 35 (2015) 795–801.

[75] S.M. Sarathy, P. Oßwald, N. Hansen, K. Kohse-Höinghaus, Alcohol combustion chemistry, Prog. Energy Combust. Sci. 44 (2014) 40-102.

[76] A. Alfazazi, U. Niemann, H. Selim, R.J. Cattolica, S.M. Sarathy, Effects of Substitution on Counterflow Ignition and Extinction of C_3 and C_4 Alcohols, Energy Fuels 30 (2016) 6091−7.

[77] A. Konnov, Yet another kinetic mechanism for hydrogen combustion, Combust. Flame 203 (2019) 14-22.

[78] S.J. Klippenstein, From theoretical reaction dynamics to chemical modeling of combustion, Proc. Combust. Inst. 36 (2017) 77–111.

[79] M.P. Burke, S.J. Klippenstein , Ephemeral collision complexes mediate chemically termolecular transformations that affect system chemistry, Nat. Chem. 9 (2017) 1078-82.

[80] A.W. Jasper, E. Kamarchik, J.A. Miller, S.J. Klippenstein, First-principles binary diffusion coefficients for H, H2, and four normal alkanes+ N_2. J. Chem. Phys., 141 (2014) 124313.

[81] A.W. Jasper, J.A. Miller, Lennard–Jones parameters for combustion and chemical kinetics modeling from full-dimensional intermolecular potentials. Combust. Flame, 161 (2014) 101-10.

[82] X. Man, C. Tang, J. Zhang, Y. Zhang, L. Pan, Z. Huang, C.K. Law, An experimental and kinetic modeling study of n-propanol and i-propanol ignition at high temperatures, Combust. Flame 161 (2014) 644–56.

[83] P.S. Veloo, F.N. Egolfopoulos, Studies of n-propanol, iso-propanol, and propane flames, Combust. Flame. 158 (2011) 501–10.

[84] W. Li, Y. Zhang, Y. Li, C. Cao, J. Zou, J. Yang, Z. Cheng, Experimental and kinetic modeling study of n-propanol and i-propanol combustion: Flow reactor pyrolysis and laminar flame propagation, Combust. Flame 207 (2019) 171-85.

[85] Q. Li, W. Jin, Z. Huang, Laminar flame characteristics of C*1*–C_5 primary alcohol-isooctane blends at elevated temperature, Energies 9 (2016) 511.

[86] P. Versailles, G.M.G. Watson, A.C.A. Lipardi, J.M. Bergthorson, Quantitative CH measurements in atmospheric-pressure, premixed flames of C_1–C_4 alkanes, Combust. Flame 165 (2016) 109–24.

[87] M.D. Bohon, M.J. Al Rashidi, S.M. Sarathy, W.L. Roberts, Experiments and simulations of NOx formation in the combustion of hydroxylated fuels, Combust. Flame 162 (2015) 2322-36.

[88] G.M.G. Watson, P. Versailles, J.M. Bergthorson, NO formation in premixed flames of C_1-C_3 alkanes and alcohols, Combust. Flame 169 (2016) 242-60.

[89] G.M.G. Watson, P. Versailles, J.M. Bergthorson, NO formation in rich premixed flames of C1-C4 alkanes and alcohols, Proc. Combust. Inst. 36 (2017) 627-35.

[90] M.D. Bohon, T.F. Guiberti, S.M. Sarathy, W.L. Roberts, Variations in non-thermal NO formation pathways in alcohol flames, Proc. Combust. Inst. 36 (3) (2017) 3995-4002.

[91] M.D. Bohon, T.F. Guiberti, W.L. Roberts, PLIF measurements of non-thermal NO concentrations in alcohol and alkane premixed flames, Combust. Flame 194 (2018) 363-75.

[92] G. Capriolo, A.A. Konnov, Combustion of propanol isomers: experimental and kinetic modelling study, Combust. Flame, under review.

[93] A.A. Konnov, Yet another kinetic mechanism for hydrogen combustion, Combust. Flame 203 (2019) 14-22.

[94] A.A. Konnov, Implementation of the NCN pathway of prompt-NO formation in the detailed reaction mechanism, Combust. Flame 156 (2009) 2093-105.

[95] E.N. Volkov, A.A. Konnov, M. Gula, K. Holtappels, A.A. Burluka, in: Proc. European Combustion Meeting, CD Paper # 810136, Vienna Austria, April 14-17 2009, p. 6.

[96] M. Abian, M.U. Alzueta, P. Glarborg, Formation of NO from N_2/O_2 Mixtures in a Flow Reactor: Toward an Accurate Prediction of Thermal NO, Int. J. Chem. Kinet. 47 (8) (2015) 518-32.

[97] A. Burcat, B. Ruscic, Third millenium ideal gas and condensed phase thermochemical database for combustion (with update from active thermochemical tables), Report No. ANL-05/20, Argonne National Lab. (ANL), 2005.

[98] W.K. Metcalfe, S.M. Burke, S.S. Ahmed, H.J. Curran, A Hierarchical and Comparative Kinetic Modeling Study of C_1-C_2 Hydrocarbon and Oxygenated Fuels, Int. J. Chem. Kinet. 45 (2013) 638-75.

[99] M. Pelucchi, M. Bissoli, C. Rizzo, Y. Zhang, K. Somers, A. Frassoldati, H. Curran, T. Faravelli, A Kinetic Modelling Study of Alcohols Operating Regimes in a HCCI Engine, SAE Int. J. Engines 10 (5) (2017) 2354−70.

[100] D. Nativel, M. Pelucchi, A. Frassoldati, A. Comandini, A. Cuoci, E. Ranzi, N. Chaumeix, T. Faravelli, Laminar flame speeds of pentanol isomers: an experimental and modeling study, Combust. Flame 166 (2016) 1-18.

[101] Y. Song, L. Marrodán, N. Vin, O. Herbinet, E. Assaf, C. Fittschen, A. Stagni, T. Faravelli, M.U. Alzueta, F. Battin-Leclerc, The sensitizing effects of NO_2 and NO on methane low temperature oxidation in a jet stirred reactor, Proc. Combust. Inst. 37 (1) (2019) 667-75.

[102] C.P. Fenimore, Formation of nitric oxide in premixed hydrocarbon flames, Proc. Combust. Inst. 13 (1971) 373–80.

[103] A.N. Hayhurst, I.M. Vince, Nitric-oxide formation from N_2 in flames: the importance of “prompt” NO, Prog. Energy Combust. Sci. 6 (1980) 35–51.

Printed by Media-Tryck, Lund 2020 NORDIC SWAN ECOLABEL 3041 0903

Faculty of Engineering
Department of Physics
Division of Combustion Physics

Lund Reports on Combustion Physics, LRCP 226
ISRN LUTFD2/TFCP-226-SE
ISBN 978-91-7895-504-6
ISSN 1102-8718